

Towards hydrogen-rich ionic $(\text{NH}_4)(\text{BH}_3\text{NH}_2\text{BH}_2\text{NH}_2\text{BH}_3)$ and related molecular $\text{NH}_3\text{BH}_2\text{NH}_2\text{BH}_2\text{NH}_2\text{BH}_3$ [#]

Rafał Owarzany^{*a}, Tomasz Jaroń^b, Krzysztof Kazimierzczuk^a, Przemysław J. Malinowski^a, Wojciech Grochala^a and Karol J. Fijałkowski^{*a}

Attempts of synthesis of ionic $(\text{NH}_4)(\text{BH}_3\text{NH}_2\text{BH}_2\text{NH}_2\text{BH}_3)$ using metathetical approach resulted in a mixture of the target compound and a partly dehydrogenated molecular $\text{NH}_3\text{BH}_2\text{NH}_2\text{BH}_2\text{NH}_2\text{BH}_3$ product. The mixed specimen was characterized by NMR and vibrational spectroscopies, and the crystal structure of their cocrystal was solved from powder x-ray diffraction data, and supplemented by theoretical density functional theory calculations. Despite their impressive hydrogen content, and similarly to ammonia borane, both title compounds release hydrogen substantially polluted with borazine, and traces of ammonia and diborane.

Introduction

Protic-hydridic compounds constitute one important family of solid-state hydrogen storage materials with the potential to be applied as onboard fuel systems required in the hydrogen economy. The presence of both positively and negatively charged hydrogen atoms results in the formation of a network of dihydrogen bonds governing the crystal structure and facilitating the process of thermal decomposition.¹ These features were observed and thoroughly described for ammonia borane,² metal amidoboranes,³ and further explored for NH_4BH_4 .⁴

Ammonia borane (AB) is one of the best-researched materials in this group, being an air and water insensitive solid and containing *ca.* 19.6% of hydrogen by weight.⁵ Unfortunately, AB releases only 1/3 of the stored hydrogen below 120°C.⁶ Moreover, the hydrogen released is contaminated with ammonia, diborane, borazine, aminoborane and aminodiborane, which excludes its use as a direct H_2 source for low-temperature fuel cells.⁷ Such high gravimetric H content, however, provides significant room for modifications – even if the relatively heavy elements are introduced, the system still should be able to fulfil the gravimetric DOE requirements for H storage materials (Fig. 1).⁸

Among the derivatives of AB, amidoborane salts of a general formula $\text{M}(\text{NH}_2\text{BH}_3)_n$ [abbreviated here as MAB or $\text{M}(\text{AB})_n$] constitute the largest group.^{9,10} Two dozens of mono- and bimetallic amidoborane salts have been reported. Some of them [*i.e.* KAB,¹¹ RbAB,^{12,13} CsAB,^{12,13} Mg(AB)₂,¹⁴ Ba(AB)₂,¹⁵ Al(AB)₃,¹⁶ LiAl(AB)₄,¹⁷ Li₂Mg(AB)₄,¹⁸] evolve pure H_2 upon thermal decomposition at *ca.* 100°C. Nonetheless, all these materials suffer from a lack of reversibility and relatively low hydrogen content available at moderate temperatures.^{9,10} Recently, a novel group of ammonia borane derivatives containing five-membered chain anions of a general formula $\text{M}(\text{BH}_3\text{NH}_2\text{BH}_2\text{NH}_2\text{BH}_3)$ [abbreviated here as $\text{M}(\text{B3N2})$] have

been reported.^{19–23} Among them, one can list two allotropes of Verkade's base salt^{20,21}, five alkali metal salts^{19,21,22,24,25} and four ionic liquids.²³ Although three of them [*i.e.* Li(B3N2)^{21,22}, (Bu₄N)(B3N2),²³ (Et₄N)(B3N2)²³] meet the target H wt% content and release pure hydrogen below 150°C, yet none of them fulfils all the DOE targets simultaneously.⁸

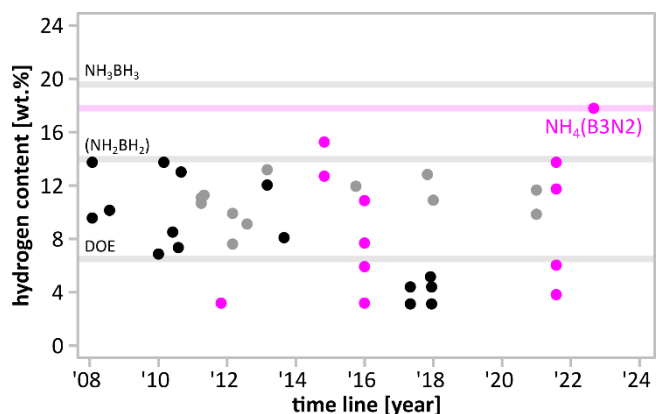


Fig. 1. Hydrogen content of monometallic amidoboranes (black), bimetallic amidoboranes (grey), $\text{M}(\text{B3N2})$ salts (magenta) as a function of reporting date. Hydrogen content of NH_3BH_3 (19.6%) polymeric (NH_2BH_2) (14.0%) and DOE ultimate target (6.5%) given as a reference.

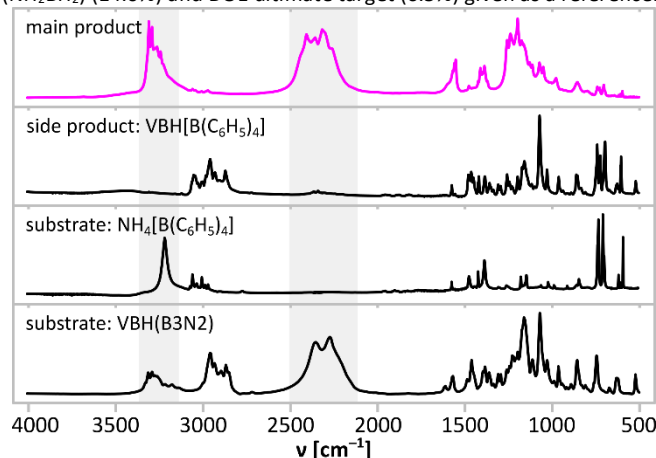


Fig. 2. Comparison of IR absorption spectra of precursors and products of metathetic synthesis performed according to Eq. 1. NH stretching and BH stretching regions are marked with grey fields.

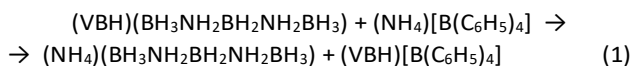
^a Centre of New Technologies, University of Warsaw
ul. Banacha 2c, 02-097 Warsaw, POLAND
^b Faculty of Chemistry, University of Warsaw
ul. Pasteura 1, 02-089 Warsaw, POLAND

[#] This work is dedicated to Prof. Roald Hoffmann at his 85th birthday
Electronic Supplementary Information (ESI) available: synthesis, NMR, FTIR, Raman, PXD, crystal structures, TGA/DSC/MS, EIS, and comparison with other ammonia borane derivatives. See DOI: 10.1039/x0xx00000x

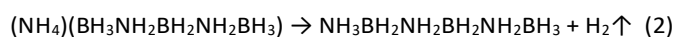
Results and discussion

2.1 Synthesis

Synthesis of $(\text{NH}_4)(\text{B3N2})$ was attempted employing Jaron's *et al.* metathetic approach mediated by the precursors containing weakly coordinating ions^{26–28}. The reaction was conducted in dry THF similarly to the previous syntheses of all alkali metal $\text{M}(\text{B3N2})$ salts²¹ according to Equation 1:



Unexpectedly, during the reaction, we observed the evolution of a small amount of gas which should not occur in a metathetic reaction. Since the expected main product contains ammonium cation and B3N2^- anion (essentially, a derivative of a borohydride anion) we assumed that – similarly to what is observed for NH_4BH_4 ²⁹ – hydrogen might be evolved upon reaction of these ions according to Equation 2:



Confirmation that this surmise is correct is presented below.

Synthesis led to a mixture of well THF-soluble products, which were separated by precipitation of the side product $(\text{VBH})[\text{B}(\text{C}_6\text{H}_5)_4]$ in dry DCM. Both products were subjected to spectroscopic analyses (Fig. 2) and powder X-ray diffraction (Fig. 3) to demonstrate successful ion exchange according to Eq. 1. Indeed, FTIR spectra (Fig. 2) of the products show that the target product contains the NH and BH groups, while the side product contains the CH groups. Unfortunately, complete separation of the main product and side product was not achieved, as documented by very weak CH bands at *ca.* 3000 cm^{-1} from $\text{B}(\text{C}_6\text{H}_5)_4^-$ anions for the former, and very weak BH bands at *ca.* 2400 cm^{-1} from $(\text{B3N2})^-$ anions for the latter product. X-ray

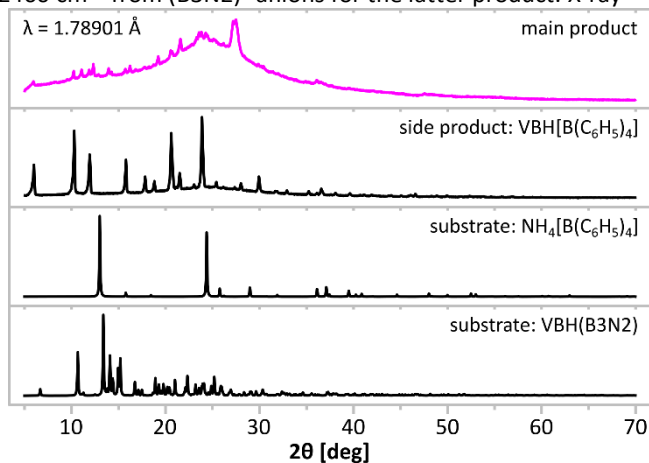


Fig. 3. Comparison of powder X-ray diffraction patterns of precursors and products of metathetic synthesis performed according to Eq. 1. $\text{CoK}_{\alpha 1,2}$, $\lambda = 1.78901\text{ \AA}$.

diffraction points to the same conclusion, showing that two new distinct crystalline species formed during the reaction (Fig. 3). The diffraction patterns of the products are free from reflections coming from the substrates which suggests at least 95% purity of the former.

2.2 NMR spectra

A detailed ^{11}B NMR investigation of the main product dissolved in THF-d_8 was performed (Fig. 4). A typical spectrum of $\text{M}(\text{B3N2})$ salt consists of a triplet at *ca.* -8.5 ppm from $[\text{BH}_2]$ groups and a quartet at *ca.* -22.5 ppm from $[\text{BH}_3]$ groups, having a relative intensity of 1:2.^{20,21} Here, the spectrum of the main product is more complicated and contains two triplets ($\delta = -10.4\text{ ppm}$, $J = 101\text{ Hz}$; $\delta = -12.3\text{ ppm}$, $J = 102\text{ Hz}$) and a quartet ($\delta = -22.2\text{ ppm}$, $J = 91\text{ Hz}$) in an intensity ratio that varies from batch to batch (in average *ca.* 4:3:5). These features altogether suggest that the main product formed according to (Eq. 1) partially undergoes a subsequent dehydrogenation reaction (Eq. 2). Variation in the observed intensity ratio of the signals may be caused by the partial decomposition of the main product thus changing the ratio between the components of the product. We note that a 1:3 mixture of $(\text{NH}_4)(\text{B3N2})$ and $\text{NH}_3\text{BH}_2\text{NH}_2\text{BH}_2\text{NH}_2\text{BH}_3$ (abbreviated as N3B3) would yield 4 BH_2 triplets units coordinated by two NH_2 groups, 3 BH_2 triplets from units coordinated by NH_2 and NH_3 , and 5 BH_3 quartets altogether. This result would suggest that *ca.* $\frac{3}{4}$ of $(\text{NH}_4)(\text{B3N2})$ decomposed to N3B3 while dissolved in THF.

To get more insights into the processes occurring during the synthesis, we conducted *in situ* $^{11}\text{B}\{^1\text{H}\}$ NMR measurements in THF-d_8 to monitor signals of the products and substrates (Fig. 5). The monitoring showed that all three signals from the product(s) (marked with #) arise simultaneously, testifying to the simultaneous progress of reactions described by Eq.1 and Eq.2. Apart from the signals assigned to the substrates and the main product, numerous additional signals which do not change during the reaction are present. These signals come from the moieties that do not play a direct role in the formation of the main product, *e.g.* $[\text{B}(\text{C}_6\text{H}_5)_4]^-$, in which the chemical neighbourhood of boron atom does not change during the

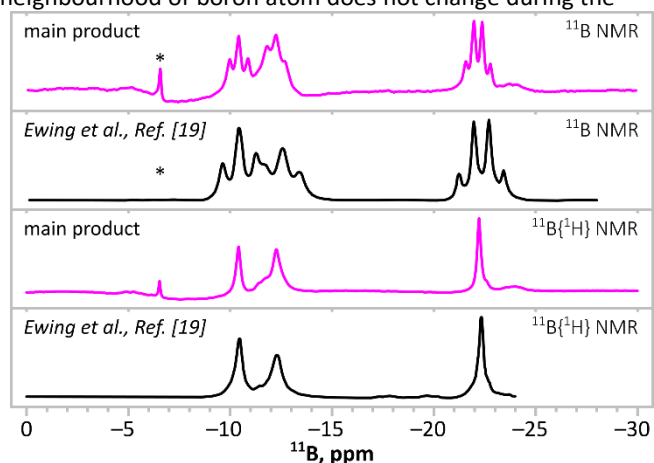
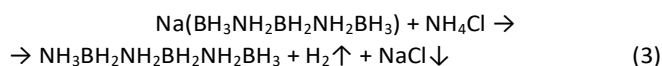


Fig. 4. Comparison of ^{11}B NMR spectra of the main product of the synthesis according to Eq. 1 (magenta lines) with the spectra of a product of reaction according to Eq. 2 reported by Ewing *et al.*¹⁹ (black lines) both with (bottom spectrum). Boron spectra show with and without ^1H decoupling. * indicates $[\text{B}(\text{C}_6\text{H}_5)_4]^-$ anions.

synthesis. The monitored reaction (Fig. 4) was not completed (*i.e.* signals of the substrates were still intense) because of the local depletion of the substrates (no mixing was applied in an NMR test tube inside the spectrometer).

It is worth mentioning that ^{11}B NMR spectrum of the main product(s) is very similar to the spectrum reported by Ewing *et al.* in 2013, having the same pattern of three signals: two triplets ($\delta = -10.5$ ppm, $J = 95$ Hz; $\delta = -12.4$ ppm, $J = 104$ Hz) and a quartet ($\delta = -22.3$ ppm, $J = 95$ Hz)¹⁹ with 4.1:3.2:5.0 intensity ratio of the signals (according to our analysis of graphical data show in that study, Fig. 9a in Ref. [19]). The report of Ewing *et al.* focused on the synthesis of a neutral 6-membered chain molecule, B3N3, via a direct reaction between Na(B3N2) and ammonium chloride, according to the following equation:¹⁹



The reaction, performed in glyme solution, was accompanied by evolution of hydrogen gas, which is similar to our observations.

Ewing *et al.* assumed that the solid product obtained was B3N3 based only on an NMR study of this material.¹⁹ Three signals observed were assigned to three boron-containing groups present in the molecule (two BH_2 , one BH_3). In the case of successful synthesis of B3N3, however, all signals observed

Table 1. Chemical shifts, J-coupling values and assignment of the signals observed in ^{11}B NMR spectra of the main product, sample reported by Ewing *et al.*¹⁹. Data for alkali metal M(B3N2) salts²¹ given as reference.

compound	-NH ₂ -BH ₂ -NH ₂ -		NH ₃ -BH ₂ -NH ₂ -		BH ₃ -NH ₂ -	
	δ [ppm]	J [Hz]	δ [ppm]	J [Hz]	δ [ppm]	J [Hz]
main product	-10.4	101	-12.3	102	-22.2	91
Ewing <i>et al.</i> ¹⁹	-10.5	95	-12.4	104	-22.3	95
(VBH)(B3N2) ²¹	-8.2	100	-	-	-21.6	91
Li(B3N2) ²¹	-8.4	103	-	-	-22.6	90
Na(B3N2) ²¹	-8.7	99	-	-	-22.4	91
K(B3N2) ²¹	-8.6	101	-	-	-22.0	89
Rb(B3N2) ²¹	-8.4	100	-	-	-21.7	90
Cs(B3N2) ²¹	-8.4	101	-	-	-21.2	94

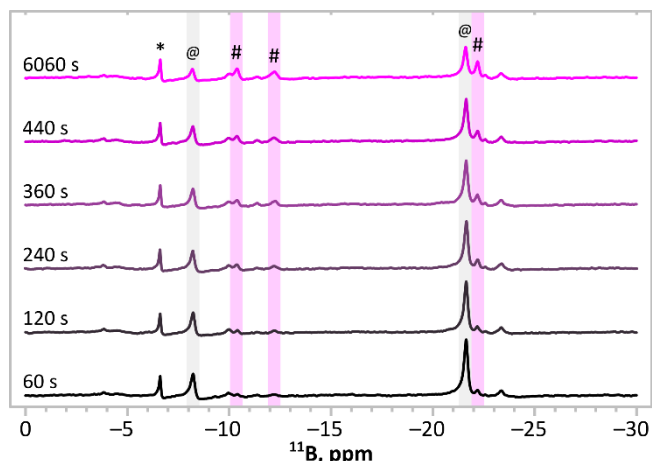


Fig. 5. The sequence of $^{11}\text{B}\{^1\text{H}\}$ NMR spectra collected *in situ* upon synthesis according to Eq. 1. The bottom spectrum shows the mixture of substrates ($t=60$ s). The top spectrum shows the final mixture of products and substrates ($t=6060$ s). @ indicates signals from substrates. # indicates signals of the main product. * indicates $[\text{B}(\text{C}_6\text{H}_5)_4]^-$ anions.

should be equally intense (1:1:1) while their intensity ratio was clearly different (Fig. 4). Our analysis suggest that the reaction towards B3N3 is in fact a two-step process (Eqn. 1 and 2) and some $(\text{NH}_4)(\text{B3N2})$ intermediate (i.e. our main target

compound) remains. The resulting assignment of NMR signals for both products is given in Table 1.

To further support our claim, we performed further characterisation of the reaction product.

2.3 FTIR and Raman analysis

Two preeminent sets of bands in the vibrational (IR absorption and Raman scattering) spectra of the main product (Fig. 6, Fig. 7), originate from stretching vibrations of NH (3000–3400 cm^{-1}) and BH (2150–2400 cm^{-1}) groups. They are accompanied by bands coming from deformation vibrations of NH_x moieties (1400–1600 cm^{-1}) as typical of M(B3N2) salts and by BN stretching. BH_x deformation modes fall below 1350 cm^{-1} .

Aside from the bands typical for M(B3N2) salts, the NH stretching region of Raman spectrum (Fig. 7) contains a relatively low frequency band (peaking at 3041 cm^{-1}) originating from ammonium cations. The ammonium cations are known to give strong Raman at much lower energies than the $[\text{NH}_2]$ and $[\text{NH}_3]$ groups, e.g. ammonium chloride gives a single band at 3052 cm^{-1} ,³⁰ while ammonium borohydride yields two bands at somewhat higher energies of 3118 cm^{-1} and 3178 cm^{-1} .^{4,31}

In the higher energy part of NH stretching region, in both FTIR and Raman spectra, we observe at least 6 distinct bands, four of which (3306 cm^{-1} , 3288 cm^{-1} , 3259 cm^{-1} , 3239 cm^{-1} in IR; 3307 cm^{-1} , 3288 cm^{-1} , 3260 cm^{-1} , 3240 cm^{-1} in Raman) form a doublet of doublets seen for heavy alkali metal M(B3N2) salts; it is characteristic for M(B3N2) salts that that the higher energy doublet is more intense in FTIR spectra, while the lower-wavenumber one is stronger in Raman spectra. In contrast, the lower energy one is more intensive in Raman spectra.²¹ The presence of such doublets is caused by Davydov splitting,³² i.e. the interaction of $[\text{NH}_2]$ groups coexisting within one crystallographic unit cell (the resonance of the corresponding

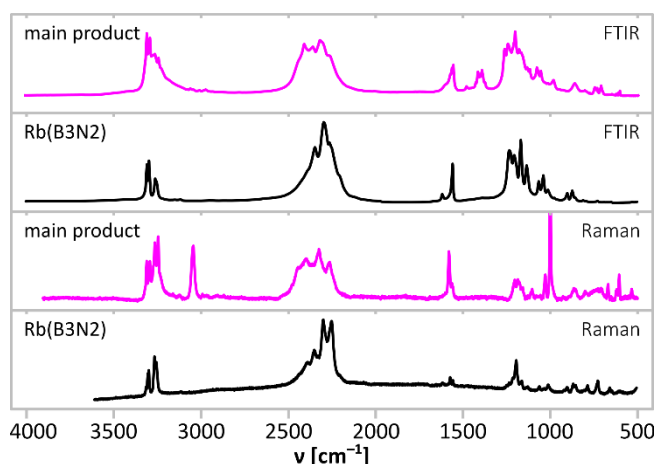


Fig. 6. Comparison of FTIR absorption (top in each bracket) and Raman scattering (bottom in each bracket) spectra of the main product of the synthesis according to Eq. 1 (magenta) and the spectra of alkali metal M(B3N2) salts. Regions magnified in Fig. 7 (NH stretching and NH bending) are marked with grey fields.

oscillators removing their degeneration). A similar split of NH band was observed in the spectra of Rb(B3N2) and Cs(B3N2), which contain gauche-form of $(\text{B3N2})^-$ anions, unlike the lighter analogues featuring straight anions and not showing Davydov

split.²¹ The split observed here equals $\pm 9\text{ cm}^{-1}$, which is intermediate between those of $\pm 4\text{ cm}^{-1}$ and $\pm 14\text{ cm}^{-1}$ seen for Rb(B3N2) and Cs(B3N2), respectively.²¹

Two remaining bands observed in NH stretching region (3224 cm^{-1} and 3268 cm^{-1} in IR), are weaker than the doublets of doublets, and they must originate from vibrations of terminal [NH₃] groups of B3N3. Indeed, they fall in a spectral region typical for terminal [NH₃] groups of ammonia borane (3196 cm^{-1} , 3253 cm^{-1} and 3311 cm^{-1}). Naturally, it is expected that signals originating from the terminal [NH₃] of B3N3 are weaker than those from more numerous [NH₂] groups present in both (NH₄)(B3N2) and B3N3.

The region of the IR absorption spectrum associated with deformations of the NH_x moieties (Figure 7) is consistent with these conclusions. One can clearly distinguish signals at *ca.* $1530\text{--}1600\text{ cm}^{-1}$, typical for [NH₂] and [NH₃] groups,²¹ from the signals at *ca.* $1250\text{--}1500\text{ cm}^{-1}$, characteristic for ammonium cations (*cf.* 1402 cm^{-1} for NH₄Cl).³³ It is worth to notice, that the IR spectra in the $1350\text{--}1500\text{ cm}^{-1}$ region show five bands (1374 cm^{-1} , 1392 cm^{-1} , 1415 cm^{-1} , 1427 cm^{-1} , 1479 cm^{-1}), and this agrees with the number of deformation modes expected for NH₄⁺ cation in a low-symmetry environment.

The spectroscopic analysis clearly shows that both (NH₄)(B3N2) and B3N3 moieties constitute the main product, thus confirming the reactions according to Eq. 1 and Eq. 2.

2.4 Crystal structure of the side product

The chemical composition of the side product of metathesis was confirmed by single crystal x-ray diffraction measurements (*cf.* ESI). This compound contains protonated Verkade's base cations and tetraphenylborate anions, (VBH)[B(C₆H₅)₄], proving successful ion exchange in reaction according to Eq. 1. The compound crystallises in $P\bar{1}$ space group with the constituent

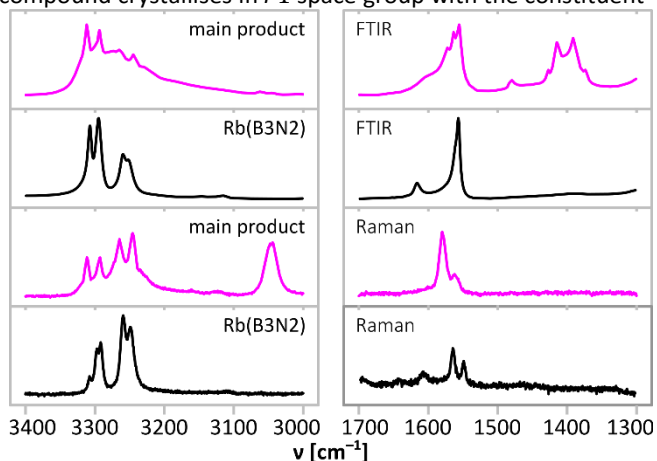


Fig. 7. Comparison of NH stretching ($3000\text{--}3400\text{ cm}^{-1}$) and NH bending ($1300\text{--}1700\text{ cm}^{-1}$) regions of FTIR absorption (top in each bracket) and Raman scattering (bottom in each bracket) spectra of the main product of the synthesis according to Eq. 1 (magenta) and alkali metal M(B3N2) salts. Full spectra presented in Fig. 6.

ions of different polarities showing no significant interactions, as expected for large ions with small charge smeared over the entire ion.

2.5 Crystal structure of the main product

As we could not obtain a single crystal of the main product, we were forced to use powder X-ray diffraction (PXRD), supported by DFT calculations and the results of spectroscopic analysis described above.

Indexing of the PXRD pattern leads to a $P2_1/c$ unit cell with the refined lattice parameters of: $a = 13.391(10)\text{ \AA}$, $b = 13.195(8)\text{ \AA}$, $c = 17.822(12)\text{ \AA}$, $\beta = 125.86(4)^\circ$ and $V = 2552(3)\text{ \AA}^3$. Assuming (NH₄)(B3N2) as a product, such unit cell volume would suggest $Z = 16$ (multiplicity of the general atomic position) and $V/Z = 159.5\text{ \AA}^3$. However, this V/Z value is too small as the values for K and Rb analogues are larger (167.7 \AA^3 and 174.3 \AA^3 respectively)²¹ while the size of NH₄⁺ falls between these two alkali metal cations. Somewhat smaller than expected V/Z volume suggests that the crystalline phase should contain also the partially dehydrogenated molecules of the product of condensation presented in Eq. 2.

To test such scenario, structural models were derived for (NH₄)(B3N2), B3N3 and the (NH₄)(B3N2)·3(B3N3) cocrystal with the components in the 1:3 molar ratio as indicated by NMR data. Initial positions of heavy atoms came from simulated annealing using the experimental diffraction data. The models were then fully optimized using periodic DFT calculations (Table 2 and SI). The theoretical unit cell volume calculated for (NH₄)(B3N2) is significantly larger than those for the models containing B3N3 moieties and the latter are only 4.0–4.5% larger than the experimental value. This degree of overestimation is rather typical for the GGA calculations.

Importantly, the closest H··H contacts in the optimized structure of (NH₄)(B3N2) remain unreasonably short (1.40 \AA), and outside the distribution observed experimentally for the dihydrogen bonds (usually $>1.80\text{ \AA}$), Fig. 9. This reconfirms that the main product is not a pure (NH₄)(B3N2). The minimum H··H contacts in the optimized crystal structures containing B3N3 are significantly longer ($1.60\text{--}1.68\text{ \AA}$), and closer to typical values for very strong dihydrogen interactions. Therefore, we have used a theoretical model of the (NH₄)(B3N2)·3(B3N3) cocrystal to refine its crystal structure using the best experimental dataset, Figure 8 and Figure S9.3 (SI).

The obtained structural model of (NH₄)(B3N2)·3(B3N3) contains four formula units in the unit cell ($Z = 4$) with one asymmetric unit ($Z' = 1$).

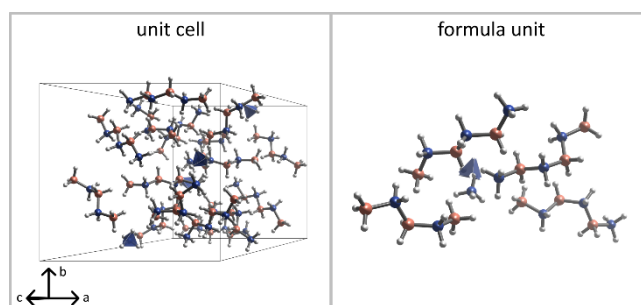


Fig. 8. Visualisation of the unit cell (left) and the asymmetric unit (right) of the crystal structure of the cocrystal comprising one unit of (NH₄)(B3N2) salt and three independent units of B3N3 molecules. Atom code: nitrogen – blue, boron – green, hydrogen – white.

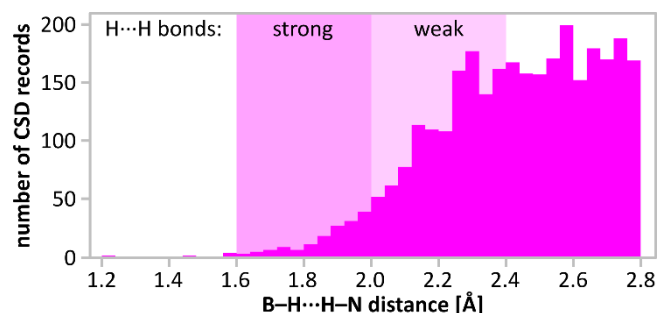


Fig. 9. Distribution of H...H distances in -B-H...H-N- moieties found in CSD database search (accessed by the end of 2020). The distances <2.8 Å were found for 865 crystal structures. Note the distances: 2.4 Å (double H van der Waals radius)¹ and 1.92 Å present in the structure.

The structure is stabilized by strong dihydrogen interactions. Two B3N3 chains adopt gauche geometry, and resemble the B3N2 anions in the heavier M(B3N2) salts, M = Rb, Cs.²¹ The third B3N3 moiety and (B3N2)⁻ anion are more straight, closer to the geometry of anionic moieties in the light M(B3N2) salts, M = Li-K.^{21,22} The B-N distances of 1.56(2)–1.58(2) Å remain within range observed in other compounds from this group. Further improvements of our preliminary experimental structure model, and in particular positions of hydrogen atoms, would require application of neutron diffraction methods, and is beyond the scope of this work.

2.6 Thermal decomposition

The theoretical gravimetric hydrogen content of the 1:3 cocrystals is very large, 16.4%. We have studied thermal decomposition of this new compound to assess its hydrogen storage properties. In Fig. 10 we present the results of a simultaneous thermogravimetric and calorimetric analysis of the main product together with gas evolution curves (hydrogen, ammonia, diborane, borazine) acquired in mass spectrometry experiment of the evolved gases.

The main product is thermally stable below 50°C. At higher temperatures, one can observe a multistep exothermic decomposition preceded by an endothermic process. During decomposition, a mixture of gases containing borazine, hydrogen, diborane and ammonia is being evolved. Close analysis of TGA/DSC/MS curves suggests that decomposition proceeds in at least 3 steps below 200°C, but each of them seems to have a similar profile of evolved gases. Interestingly, borazine is the main gaseous product of thermal decomposition, just as in the case of NH₃BH₃,⁶ but dissimilarly to alkali metal M(B3N2) salts.^{21,22} Facile evolution of borazine

Table 2. Summary of the DFT results. Minimum H...H distance is given for fully optimized unit cell and those which lattice vectors were fixed at experimental values. The model of (NH₄)(B3N2)-3(B3N3) refined to the experimental XRD data is added for comparison.

Compound	V [Å ³]	ΔV [%]	d(H...H) _{min} cell opt. [Å]	d(H...H) _{min} cell fix [Å]
NH ₄ (B3N2)	2832.0	11.0	1.40	1.42
(NH ₄)(B3N2)-3(B3N3)	2666.1	4.5	1.60	1.62
	2552.2(30)*	–	1.92*	–
B3N3	2654.7	4.0	1.68	1.65

* Experimental data with the lower constrain on the H...H separation.

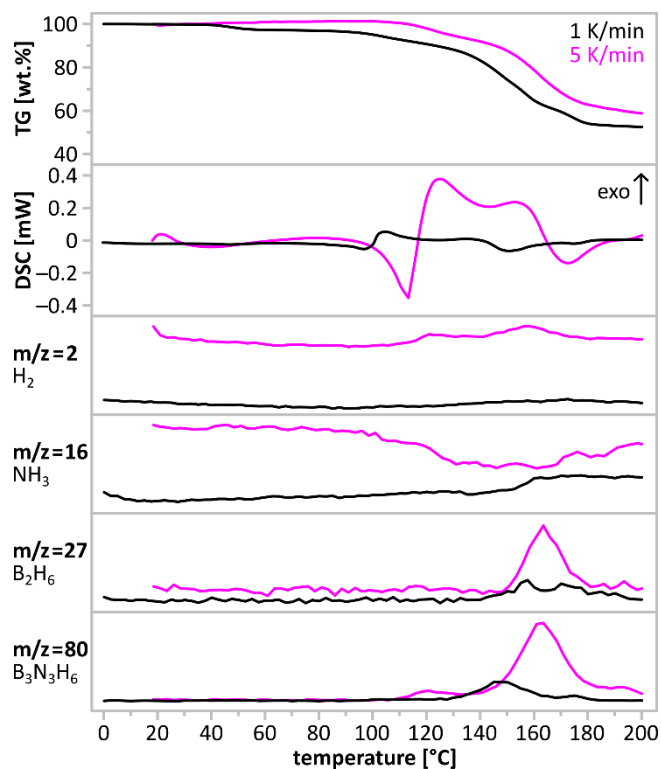
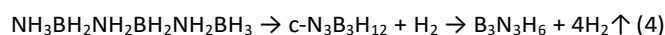


Fig. 10. Thermogravimetric (TG) and calorimetric (DSC) profiles of the main product set together with MS profiles of the evolved volatile products: hydrogen (m/z = 2), ammonia (m/z = 16), diborane (m/z = 27), borazine (m/z = 80). Scanning rate: 1 K/min (black), 5 K/min (magenta).

may be related to stoichiometry of two components of the main product. (NH₄)(B3N2) and B3N3, both contain 3 boron atoms and 3 nitrogen atoms, just like borazine molecules. Dehydrogenation of B3N3 molecule proceeds with formation of a new B-N bond at [BH₃] and [NH₃] terminals according to Eq. 4. This reaction was also proposed as the final step of borazine evolution during thermal decomposition of ammonia borane.³⁴ Formation of pseudo-aromatic borazine is accompanied by dehydrogenation of the elusive head-to-tail cyclohexane-like intermediates, according to Equation 4.



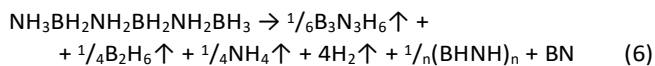
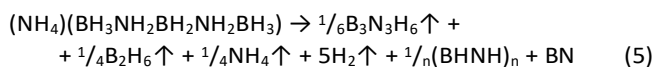
We also observed the formation of B₂H₆ and NH₃, similarly as in decomposition of Na(B3N2),^{21,22} K(B3N2),²¹ Rb(B3N2)²¹ and Cs(B3N2),²¹ which come from fragmentation of (B3N2)⁻ anions.

As mentioned above, the thermal decomposition of the main product is preceded by an endothermic process. Analogies to ammonia borane⁶ and amidoboranes¹⁰ might suggest melting of the sample. However, direct visual observations ruled out this possibility. Endothermic event is related either to an intermolecular reorganization or a structural phase transition.

Depending on the heating rate, decomposition temperature reaches the fastest rate at ca. 145°C ca. 152°C for 1 K/min and 5 K/min scans, respectively. The observed mass loss upon thermal decomposition in the range up to 200°C, equals ca. 45% and surpasses those of alkali metal M(B3N2) salts²¹ and parent ammonia borane.⁶ Such large observed mass loss may be attributed to the evolution of borazine and other volatiles. The

solid residue is amorphous, and consists of boron nitride and polymeric $B_xN_yH_z$ phases as deduced from FTIR analysis (cf. ESI).

The observations discussed above lead to the following overall equations describing thermal decomposition of the two components of the main product:



Theoretical mass loss of Eq. 5 and Eq.6 equal 43% and 42%, respectively, which reasonably agree with the observed experimental mass loss of ca. 45%.

Conclusions

Synthesis of hydrogen-rich $(NH_4)(B_3N_2)$ salt was attempted in metathetic approach using precursors which contained weakly coordinating ions. The obtained product, however, corresponds to a mixture of ionic $(NH_4)(B_3N_2)$ and neutral B_3N_3 forming cocrystals in molar ratio of 1:3. Based on available ^{11}B NMR data, the main product was found to be very similar to the samples reported earlier by Ewing *et al.*¹⁹ as B_3N_3 .

The compound crystallises in $P2_1/c$ unit cell with the lattice parameters of: $a = 13.401(11)$ Å, $b = 13.196(8)$ Å, $c = 17.828(12)$ Å, $\beta = 128.83(4)^\circ$, $V = 2556(3)$ Å³ and $Z = 16$. The expected side product of a metathetic reaction, $(VBH)[B(C_6H_5)_4]$, crystallises in $P\bar{1}$ unit cell with the lattice parameters of $a = 11.7376(3)$ Å, $b = 19.5388(5)$ Å, $c = 20.5479(4)$ Å, $\alpha = 61.751(2)^\circ$, $\beta = 73.618(2)^\circ$, $\gamma = 89.605(2)^\circ$, $V = 3937.71$ Å³ and $Z = 4$.

Despite its high hydrogen content of 16.4%, the new compound cannot act as a self-standing solid-state hydrogen reservoir as it decomposes via a set of exothermic events while evolving mixture of volatile gaseous products such as borazine, diborane and ammonia, aside from hydrogen. However, it is possible that templating our product in porous matrixes could result in substantial improvement of purity of the evolved hydrogen, similarly as it was observed for ammonia borane.³⁵

Experimental

Reagents: All operations were performed under inert Ar atmosphere inside gloveboxes, MBRAUN Labmaster DP or Vigor SG1200 (O_2 , $H_2O < 1.0$ ppm). Commercially available reagents and solvents were used: NH_3BH_3 (98%, JSC Aviator), $NH_4B(C_6H_5)_4$ (99%, Sigma-Aldrich (later denoted as SA)), C_4H_8O (99%, SA), CH_2Cl_2 (99%, SA). The synthesis of $(C_{18}H_{39}N_4PH)(BH_3NH_2BH_2NH_2BH_3)$ was performed according to the route described in our earlier paper.²¹ For NMR measurements we used THF-d₈ (99.5 atom% D, SA).

Infrared absorption spectroscopy: FTIR spectra were measured in the standard range of 400–4000 cm^{-1} using Fourier Transform IR spectrometer Vertex 80v from Bruker. Samples were examined using KBr pellets prepared using anhydrous KBr (99%, SA) additionally dried in 150°C for 24h.

Raman spectroscopy: Raman scattering measurements were done using Raman microscopy setup from Jobin Yvon T64000 with Si CCD detector and Kr-Ar gas laser from

Spectraphysics. We used green 514.5 nm excitation line. For the measurements small doses of samples were placed in 0.5 mm thick quartz capillaries sealed under inert gas atmosphere.

Nuclear Magnetic Resonance: ^{11}B NMR spectra with and without 1H decoupling were obtained using Agilent 700 MHz spectrometer with Direct Drive 2 console and 5 mm room-temperature broadband probe. We used deuterated tetrahydrofuran (d_8 -THF) as a solvent. The number of scans has been set to 256, the interscan delay to 1 s and the acquisition time to 200 ms. The spectra were acquired at 25 C. The exponential apodization has been used during processing (line broadening of 5 Hz).

Thermogravimetric Analysis: Thermal decomposition was investigated using STA 410 thermal analyser from Netzsch, in the temperature range from $-10^\circ C$ to $+200^\circ C$. STA 449 allows simultaneous thermogravimetric analysis, differential scanning calorimetry and evolved gas analysis by means of mass spectrometry. The samples were loaded into alumina crucibles inside a glovebox. Helium was used as a carrier gas. Evolved gases were analysed with a QMS 403C Aëolos MS from Pfeiffer–Vacuum. Transfer line was preheated to 100°C to avoid condensation of residues.

Powder X-ray diffraction: PXRD measurements were conducted on samples sealed in 0.5 mm thick quartz capillaries under inert atmosphere. Two diffractometers were used: Panalytical X'Pert Pro with linear PIXcel Medipix2 detector (parallel beam; the $CoK\alpha_{12}$ radiation); and Bruker D8 Discover with 2D Vantec detector (parallel beam; the $CuK\alpha_{12}$ radiation).

Crystal structure solution of the main product: Diffraction signals have been indexed using X-cell³⁶ and the initial structural model has been obtained using FOX software,³⁷ while the Rietveld refinement has been performed in Jana2006.³⁸ Pseudovoigt functions with Berrar-Baldinozzi asymmetry have been used for modeling of diffraction profiles. The restraints were used during refinement for the N–H and B–H distances (at 0.900(10) Å and 1.100(10) Å, respectively, Fig. S9.2), and the angles related to hydrogen atoms (to 109.47° with tolerance of ca. 0.5°). The N–B distances were set to the value 1.57(1) Å. The atomic displacement parameters of B and N atoms were set equal, while those of H atoms were constrained according to the riding model. The bottom constraint of 1.91 Å for H...H distances was applied. Further details on the crystal structure may be obtained from CCDC/FIZ Karlsruhe on quoting the CSD deposition No. 2193624.

Crystal structure solution of the side product: Crystal of the compound were covered with perfluorinated oil (Krytox 1531). Data collection and reduction was performed with Agilent Supernova X-ray diffractometer with $K\alpha$ -Cu radiation (microsource) with data reduction performed by CrysAlisPro software (v. 40.99).³⁹ Structure solution: SHELXT,⁴⁰ refinement against F^2 in Shelxl-2018, with ShelXle as GUI software.⁴¹ The disorder of the $-OC(CF_3)_3$ groups was resolved using DSR.⁴² Further details on the crystal structure may be obtained from CCDC/FIZ Karlsruhe on quoting the CSD deposition No. XXX.

Density Functional Theory (DFT) calculations were performed using CASTEP.⁴³ Generalized Gradient Approximation (GGA) was used with PBE functional and

Tkatchenko-Scheffler dispersive correction.⁴⁴ The cutoff value of 500 eV was applied to achieve good energy convergence. The density of the k-point grid was set below 0.1 Å⁻¹ and ultrasoft, generated on the fly pseudopotentials were used as they provide more accurate lattice parameters.

Graphical presentation of crystal structures has been performed with Vesta.⁴⁵

Conflicts of interest

There are no conflicts of interests to declare.

Acknowledgements

This research was funded by Polish National Science Centre within the projects Preludium 13 (UMO/2017/25/N/ST5/01977) and Sonata Bis 8 (UMO/2018/30/E/ST5/00854). Research was carried out with the use of CePT infrastructure financed by the European Union – the European Regional Development Fund within the Operational Programme "Innovative economy" for 2007–2013 (POIG.02.02.00-14-024/08-00).

Notes and references

Supplementary Information (ESI) contains detailed data for the main product and reference data for M(BH₃NH₂BH₂NH₂BH₃) salts.

- 1 T. Richardson, S. de Gala, R. H. Crabtree and P. E. M. Siegbahn, *J Am Chem Soc*, 1995, **117**, 12875–12876.
- 2 W. T. Klooster, T. F. Koetzle, P. E. M. Siegbahn, T. B. Richardson and R. H. Crabtree, *J Am Chem Soc*, 1999, **121**, 6337–6343.
- 3 E. Magos-Palasyuk, T. Palasyuk, P. Zaleski-Ejgierd and K. Fijalkowski, *CrystEngComm*, 2014, **16**, 10367–10370.
- 4 S. Filippov, J. B. Grinderslev, M. S. Andersson, J. Armstrong, M. Karlsson, T. R. Jensen, J. Klarbring, S. I. Simak and U. Häussermann, *The Journal of Physical Chemistry C*, 2019, **123**, 28631–28639.
- 5 U. B. Demirci, *Energies (Basel)*, 2020, **13**, 3071.
- 6 F. Baitalow, J. Baumann, G. Wolf, K. Jaenicke-Röblier and G. Leitner, *Thermochimica Acta*, 2002, **391**, 159–168.
- 7 A. Al-Kukhun, H. T. Hwang and A. Varma, *International Journal of Hydrogen Energy*, 2013, **38**, 169–179.
- 8 DOE Technical Targets for Onboard Hydrogen Storage for Light-Duty Vehicles.
- 9 Y. S. Chua, P. Chen, G. Wu and Z. Xiong, *Chemical Communications*, 2011, **47**, 5116.
- 10 R. Owarzany, P. Leszczyński, K. Fijalkowski and W. Grochala, *Crystals (Basel)*, 2016, **6**, 88.
- 11 H. V. K. Diyabalanage, T. Nakagawa, R. P. Shrestha, T. A. Semelsberger, B. L. Davis, B. L. Scott, A. K. Burrell, W. I. F. David, K. R. Ryan, M. O. Jones and P. P. Edwards, *J Am Chem Soc*, 2010, **132**, 11836–11837.
- 12 I. v. Kazakov, A. v. Butlak, P. A. Shelyganov, V. v. Suslonov and A. Y. Timoshkin, *Polyhedron*, 2017, **127**, 186–190.
- 13 R. Owarzany, T. Jaroń, P. J. Leszczyński, K. J. Fijalkowski and W. Grochala, *Dalton Transactions*, 2017, **46**, 16315–16320.
- 14 J. Luo, X. Kang and P. Wang, *Energy and Environmental Science*, 2013, **6**, 1018–1025.
- 15 N. A. Shcherbina, I. v. Kazakov and A. Y. Timoshkin, *Russian Journal of General Chemistry*, 2017, **87**, 2875–2877.
- 16 M. F. Hawthorne, S. S. Jalisatgi, A. v. Safronov, H. B. Lee and J. Wu, *Chemical Hydrogen Storage Using Polyhedral Borane Anions and Aluminum-Ammonia-Borane Complexes*, 2010.
- 17 G. Xia, Y. Tan, X. Chen, Z. Guo, H. Liu and X. Yu, *J. Mater. Chem. A*, 2013, **1**, 1810–1820.
- 18 N. Biliškov, A. Borgschulte, K. Užarević, I. Halasz, S. Lukin, S. Milošević, I. Milanović and J. G. Novaković, *Chemistry – A European Journal*, 2017, **23**, 16274–16282.
- 19 W. C. Ewing, P. J. Carroll and L. G. Sneddon, *Inorganic Chemistry*, 2013, **52**, 10690–10697.
- 20 W. C. Ewing, A. Marchione, D. W. Himmelberger, P. J. Carroll and L. G. Sneddon, *J Am Chem Soc*, 2011, **133**, 17093–17099.
- 21 R. Owarzany, K. J. Fijalkowski, T. Jaroń, P. J. Leszczyński, Ł. Dobrzycki, M. K. Cyrański and W. Grochala, *Inorganic Chemistry*, 2016, **55**, 37–45.
- 22 K. J. Fijalkowski, T. Jaroń, P. J. Leszczyński, E. Magos-Palasyuk, T. Palasyuk, M. K. Cyrański and W. Grochala, *Phys. Chem. Chem. Phys.*, 2014, **16**, 23340–23346.
- 23 X. Chen, X. Jiang, Y. Jing and X. Chen, *Chemistry – An Asian Journal*, 2021, **16**, 2475–2480.
- 24 I. C. Evans, Dissertation, University of Birmingham, 2011.
- 25 K. R. Ryan, Dissertation, University of Oxford, 2011.
- 26 A. Starobrat, M. J. Tyszkiewicz, W. Wegner, D. Pancerz, P. A. Orłowski, P. J. Leszczyński, K. J. Fijalkowski, T. Jaroń and W. Grochala, *Dalton Transactions*, 2015, **44**, 19469–19477.
- 27 T. Jaroń, W. Wegner, K. J. Fijalkowski, P. J. Leszczyński and W. Grochala, *Chemistry - A European Journal*, 2015, **21**, 5689–5692.
- 28 T. Jaroń, P. A. Orłowski, W. Wegner, K. J. Fijalkowski, P. J. Leszczyński and W. Grochala, *Angewandte Chemie - International Edition*, 2015, **54**, 1236–1239.
- 29 R. W. Parry, D. R. Schultz and P. R. Girardot, *J Am Chem Soc*, 1958, **80**, 1–3.
- 30 R. S. Krishnan, *Proceedings of the Indian Academy of Sciences - Section A*, 1947, **26**, 432.
- 31 A. Karkamkar, S. M. Kathmann, G. K. Schenter, D. J. Heldebrant, N. Hess, M. Gutowski and T. Autrey, *Chemistry of Materials*, 2009, **21**, 4356–4358.
- 32 A. S. Davydov, *Theory of Molecular Excitons*, Springer, 1971.
- 33 W. E. Wallace, in *NIST Standard Reference Database Number 69*, eds. P. Linstrom and W. Mallard, National Institute of Standards and Technology, 2018.
- 34 H. Wu, W. Zhou and T. Yildirim, *J Am Chem Soc*, 2008, **130**, 14834–14839.
- 35 A. Gutowska, L. Li, Y. Shin, C. M. Wang, X. S. Li, J. C. Linehan, R. S. Smith, B. D. Kay, B. Schmid, W. Shaw, M. Gutowski and T. Autrey, *Angewandte Chemie International Edition*, 2005, **44**, 3578–3582.
- 36 M. A. Neumann, *Journal of Applied Crystallography*, 2003, **36**, 356–365.
- 37 V. Favre-Nicolin and R. Černý, *Journal of Applied Crystallography*, 2002, **35**, 734–743.
- 38 V. Petříček, M. Dušek and L. Palatinus, *Zeitschrift für Kristallographie - Crystalline Materials*, 2014, **229**, 345–352.
- 39 Agilent, 2014.
- 40 G. M. Sheldrick, *Acta Crystallographica Section A Foundations and Advances*, 2015, **71**, 3–8.

- 41 C. B. Hübschle, G. M. Sheldrick and B. Dittrich, *Journal of Applied Crystallography*, 2011, **44**, 1281–1284.
- 42 D. Kratzert, J. J. Holstein and I. Krossing, *Journal of Applied Crystallography*, 2015, **48**, 933–938.
- 43 S. J. Clark, M. D. Segall, C. J. Pickard, P. J. Hasnip, M. I. J. J. Probert, K. Refson and M. C. Payne, *Zeitschrift für Kristallographie*, 2005, **220**, 567–570.
- 44 A. Tkatchenko and M. Scheffler, *Physical Review Letters*, 2009, **102**, 073005.
- 45 K. Momma and F. Izumi, *Journal of Applied Crystallography*, 2011, **44**, 1272–1276.

ELECTRONIC SUPPLEMENTARY INFORMATION

“Towards hydrogen-rich ionic $(\text{NH}_4)(\text{BH}_3\text{NH}_2\text{BH}_2\text{NH}_2\text{BH}_3)$ and related molecular $\text{NH}_3\text{BH}_2\text{NH}_2\text{BH}_2\text{NH}_2\text{BH}_3$ ”

R. Owarzany, T. Jaroń, K. Kazimierczuk, P. J. Malinowski, W. Grochala, K. J. Fijalkowski

Contents:

1. Records of reports on novel amidoborane and $\text{M}(\text{B}_3\text{N}_2)$ salts and related compounds:
2. Synthesis of $\text{M}(\text{B}_3\text{N}_2)$ salts of the products obtained:
 $(\text{NH}_4)(\text{B}_3\text{N}_2) \cdot 3(\text{B}_3\text{N}_3)$ Li(B_3N_2) Na(B_3N_2) K(B_3N_2) Rb(B_3N_2) Cs(B_3N_2) NH_3BH_3
3. Table of ^{11}B NMR @ THF- d_8 chemical shifts of $\text{M}(\text{B}_3\text{N}_2)$ salts and ammonia borane:
 $(\text{NH}_4)(\text{B}_3\text{N}_2) \cdot 3(\text{B}_3\text{N}_3)$ Li(B_3N_2) Na(B_3N_2) K(B_3N_2) Rb(B_3N_2) Cs(B_3N_2) NH_3BH_3 VBH(B_3N_2)
4. Table of bands appearing in the FTIR spectra of $\text{M}(\text{B}_3\text{N}_2)$ salts and ammonia borane:
 $(\text{NH}_4)(\text{B}_3\text{N}_2) \cdot 3(\text{B}_3\text{N}_3)$ Li(B_3N_2) Na(B_3N_2) K(B_3N_2) Rb(B_3N_2) Cs(B_3N_2) NH_3BH_3
5. Table of bands appearing in the Raman spectra of $\text{M}(\text{B}_3\text{N}_2)$ salts and ammonia borane:
 $(\text{NH}_4)(\text{B}_3\text{N}_2) \cdot 3(\text{B}_3\text{N}_3)$ Li(B_3N_2) Na(B_3N_2) K(B_3N_2) Rb(B_3N_2) Cs(B_3N_2) NH_3BH_3
6. Comparison FTIR and Raman spectra of $\text{M}(\text{B}_3\text{N}_2)$ salts:
 $(\text{NH}_4)(\text{B}_3\text{N}_2) \cdot 3(\text{B}_3\text{N}_3)$ Li(B_3N_2) Na(B_3N_2) K(B_3N_2) Rb(B_3N_2) Cs(B_3N_2)
7. Thermal decomposition (TGA curves) of $\text{M}(\text{B}_3\text{N}_2)$ salts:
 $(\text{NH}_4)(\text{B}_3\text{N}_2) \cdot 3(\text{B}_3\text{N}_3)$ Li(B_3N_2) Na(B_3N_2) K(B_3N_2) Rb(B_3N_2) Cs(B_3N_2)
8. FTIR spectra of the products of thermal decomposition of $\text{M}(\text{B}_3\text{N}_2)$ salts:
 $(\text{NH}_4)(\text{B}_3\text{N}_2) \cdot 3(\text{B}_3\text{N}_3)$ Li(B_3N_2) Na(B_3N_2) K(B_3N_2) Rb(B_3N_2) Cs(B_3N_2)
9. Experimental crystal structure and Rietveld fit for $(\text{NH}_4)(\text{B}_3\text{N}_2) \cdot 3(\text{B}_3\text{N}_3)$:
 $(\text{NH}_4)(\text{B}_3\text{N}_2) \cdot 3(\text{B}_3\text{N}_3)$
10. Table with the closest $\text{H} \cdots \text{H}$ distances in the crystal structure of $(\text{NH}_4)(\text{B}_3\text{N}_2) \cdot 3(\text{B}_3\text{N}_3)$:
 $(\text{NH}_4)(\text{B}_3\text{N}_2) \cdot 3(\text{B}_3\text{N}_3)$
11. Experimental and modelled NMR spectra for various possible compositions of the main product:
 $(\text{NH}_4)(\text{B}_3\text{N}_2) \cdot 3(\text{B}_3\text{N}_3)$ $(\text{NH}_4)(\text{B}_3\text{N}_2)$ (B_3N_3)
12. Results of DFT optimisation of modelled crystal structures:
 $(\text{NH}_4)(\text{B}_3\text{N}_2) \cdot 3(\text{B}_3\text{N}_3)$ $(\text{NH}_4)(\text{B}_3\text{N}_2)$ (B_3N_3)
13. Crystal structure VBH)[$\text{B}(\text{C}_6\text{H}_5)_4$]
VBH)[$\text{B}(\text{C}_6\text{H}_5)_4$]

1. Records of reporting synthesis of novel amidoborane and M(B3N2) salts and related compounds:

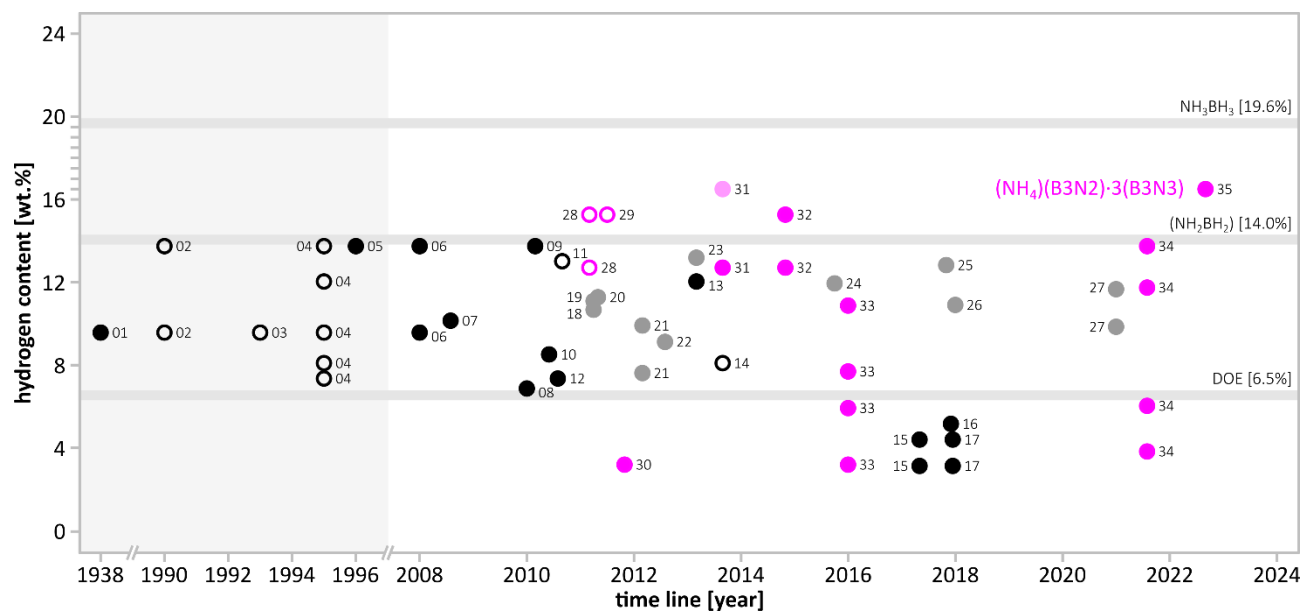


Fig. S1.1. Hydrogen content of monometallic amidoboranes (black), bimetallic amidoboranes (grey), M(B₃N₂) salts (magenta) and as a function of reporting date. Hydrogen content of NH₃BH₃ (19.6%), polymeric (NH₂BH₂) (14.0%) and DOE ultimate target (6.5%) given as a reference. Reports and these marked with hollow circles.

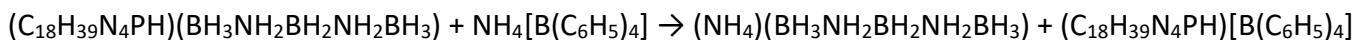
References:

- 01 NaAB (9.5%) – H. I. Schlesinger, A.B. Burg, *J. Am. Chem. Soc.* 60 (1938) 290–299.
- 02 α-LiAB (13.7%), NaAB (9.5%) – P. M. Niedenzu, *Ph.D. Thesis*, Ohio State University, 1990.
- 03 NaAB (9.54%) – T. Salupo, *Ph.D. Thesis*, Ohio State University, 1993.
- 04 α-LiAB (13.7%), NaAB (9.5%), KAB (7.3%), Mg(AB)₂ (12.0%), Zn(AB)₂ (8.1%) – A. L. DeGraffenreid, *Ph.D. Thesis*, Ohio State University, 1995.
- 05 α-LiAB (13.7%) – A. G. Myers, *et al.*, *Tetrahedron Lett.* 37 (1996) 3623–3626.
- 06 α-LiAB (13.70%), NaAB (9.54%) – Z. Xiong, *et al.*, *Nature Mater.* 7 (2008) 138–141.
- 07 Ca(AB)₂ (10.10%) – J. Spielmann, *et al.*, *Angew. Chem. Int. Ed.* 47 (2008) 6290–6295.
- 08 Sr(AB)₂ (6.84%) – Q. Zhang, *et al.*, *J. Phys. Chem. C* 114 (2010) 1709–1714.
- 09 β-LiAB (13.70%) – C. Wu, *et al.*, *Inorg. Chem.* 49 (2010) 4319–4323.
- 10 Y(AB)₃ (8.47%) – R. V. Genova, *et al.*, *J. Alloys. Comp.* 499 (2010) 144–148.
- 11 Al(AB)₃ (12.97%) – M. F. Hawthorne, *et al.*, *Final Report*, University of Missouri, 2010.
- 12 KAB (7.31%) – H. V. K. Diyabalanage, *et al.*, *J. Am. Chem. Soc.* 132 (2010) 11836–11837.
- 13 Mg(AB)₂ (12.00%) – J. Luo, *J. et al.*, *Energy Environ. Sci.* 6 (2013) 1018–1025.
- 14 Zn(AB)₂ (8.06%) – R. Owarzany, *M.Sc. Thesis*, University of Warsaw, 2013.
- 15 LT-RbAB (4.37%), LT-CsAB (3.1%) – I. V. Kazakov, *et al.*, *Polyhedron* 127 (2017) 186–190.
- 16 Ba(AB)₂ (5.12%) – N. A. Shcherbina, *et al.*, *Rus. J. Gen. Chem.* 87 (2017) 2875–2877.
- 17 HT-RbAB (4.37%), HT-CsAB (3.1%) – R. Owarzany, *et al.*, *Dalton Trans.* 46 (2017) 16315–16320.
- 18 Na₂Mg(AB)₄ (10.63%) – H. Wu, *et al.*, *Chem. Commun.* 47 (2011) 4102–4104.
- 19 NaMg(AB)₃ (11.05%) – X. Kang, *et al.*, *Dalton Trans.* 40 (2011) 3799–3801.
- 20 LiNa(AB)₂ (11.24%) – K. J. Fijalkowski, *et al.*, *Dalton Trans.* 40 (2011) 4407–4413.
- 21 KMg(AB)₃ (9.88%), RbMg(AB)₃ (7.58%) – X. Kang, *et al.*, *Int. J. Hydrog. Energy* 37 (2012) 4259–4266.
- 22 K₂Mg(AB)₄ (9.08%) – Y. S. Chua, *et al.*, *Chem. Mater.* 24 (2012) 3574–3581.
- 23 LiAl(AB)₄ (13.15%) – G. Xia *et al.*, *Mater. Chem. A.* 1 (2013) 1810–1820.
- 24 NaAl(AB)₄ (11.9%) – I. Dovgaliuk *et al.*, *Chem. Eur. J.* 21 (2015) 14562–14570.
- 25 Li₂Mg(AB)₄ (12.79%) – N. Biliškov *et al.*, *Chem. Eur. J.* 23 (2017) 16274–16282.
- 26 KAl(AB)₄ (10.87%) – K. T. Møller, *et al.*, *Int. J. Hydrog. Energy* 43 (2018) 311–321.
- 27 Li₂Ca(AB)₄ (11.63%), Na₂Ca(AB)₄ (9.81%) – I. Milanovic, *et al.*, *ACS Sustainable Chem. Eng.* 9 (2021) 2089–2099.
- 28 Li(B₃N₂) (15.22%), Na(B₃N₂) (12.66%) – I. C. Evans, *Ph.D. Thesis*, University of Birmingham, 2011.
- 29 Li(B₃N₂) (15.22%) – K. R. Ryan, *Ph.D. Thesis*, University of Oxford, 2011.
- 30 α-VB(B₃N₂) (3.15%) – W. C. Ewing, *et al.*, *J. Am. Chem. Soc.* 133 (2011) 17093–17099.
- 31 Na(B₃N₂) (12.66%), (NH₄)(B₃N₂)/3(B₃N₃) (16.4%) – W. C. Ewing, *et al.*, *Inorg. Chem.* 52 (2013) 10690–10697.
- 32 Li(B₃N₂) (15.22%), Na(B₃N₂) (12.66%) – K. J. Fijalkowski, *et al.*, *Phys. Chem. Chem. Phys.* 16 (2014) 23340–23346.
- 33 K(B₃N₂) (10.83%), Rb(B₃N₂) (7.65%), Cs(B₃N₂) (5.89%), β-VB(B₃N₂) (3.15%) – R. Owarzany, *et al.*, *Inorg. Chem.* 55 (2016) 37.
- 34 (Bu₄N)(B₃N₂) (3.80%), (Et₄N)(B₃N₂) (6.00%), [C(N₃H₆)](B₃N₂) (13.70%), [C(N₃H₅CH₃)](B₃N₂) (11.7%) – X. M. Chen, *Chem Asian J.* 16 (2021) 1–7.
- 35 (NH₄)(B₃N₂)/3(B₃N₃) (16.4%) – this study

2. Synthesis of alkali metal M(B3N2) salts:

All operations were performed under inert Ar atmosphere inside gloveboxes, MBRAUN Labmaster DP or Vigor SG1200 (O₂, H₂O < 1.0 ppm). Commercially available reagents and solvents were used: NH₃BH₃ (98%, JSC Aviabor), NH₄B(C₆H₅)₄ (99%, Sigma-Aldrich (later denoted as SA), C₄H₈O (99%, SA), CH₂Cl₂ (99%, SA).

Metathetic synthesis was performed using (C₁₈H₃₉N₄PH)(BH₃NH₂BH₂NH₂BH₃) and NH₄[B(C₆H₅)₄] in anhydrous THF at room temperature under argon atmosphere:



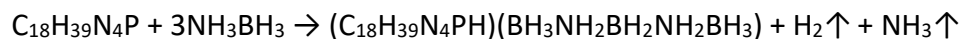
A follow-up process of dehydrogenation of NH₄(BH₃NH₂BH₂NH₂BH₃) occurs leading to neutral linear molecule NH₃BH₂NH₂BH₂NH₂BH₃:



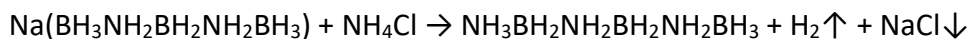
Obtained mixture of products was well soluble in THF. Side product (C₁₈H₃₉N₄PH)[B(C₆H₅)₄] was precipitated by washing with anhydrous DCM.

The main product crystallises in P2₁/c unit cell with the lattice parameters of: a = 13.401(11) Å, b = 13.196(8) Å, c = 17.828(12) Å, β = 128.83(4)°, V = 2556(3) Å³ and Z = 16. The crystalline product contains two compounds: NH₄(BH₃NH₂BH₂NH₂BH₃) and NH₃BH₂NH₂BH₂NH₂BH₃ in molar ratio 1:3. In the manuscript, the product is denoted as “main product” or “(NH₄)(B3N2)·3(B3N3)”.

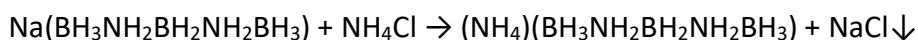
The synthesis of (C₁₈H₃₉N₄PH)(BH₃NH₂BH₂NH₂BH₃) was performed according to the route described in our earlier paper (R. Owarzany, *et al.*, *Inorg. Chem.* 55 (2016) 37/) in a direct reaction of Verkade’s Base with 3 equivalents of ammonia borane in toluene at room temperature:



Different route of metathetic synthesis between Na(BH₃NH₂BH₂NH₂BH₃) and NH₄Cl in glyme at room temperature for 24 hours was reported earlier (W. C. Ewing *et al.* *Inorg. Chem.* 52 (2013) 10690.), however, the authors were aiming NH₃BH₂NH₂BH₂NH₂BH₃ according to the following equation:



Judging from the comparison of NMR data presented by Ewing *et al.* to our own data we strongly believe that this process leads to (NH₄)(B3N2)·3(B3N3) according to the following reaction equations:



3. Table of ^{11}B NMR @ THF- d_8 chemical shifts of $\text{M}(\text{B3N2})$ salts and ammonia borane:

Table S3. Chemical shifts, positions of multiplets, excitation frequencies and J-coupling values observed in ^{11}B NMR spectra in deuterated THF solution (δ [ppm]) of $(\text{NH}_4)(\text{B3N2})\cdot 3(\text{B3N3})$ at room temperature. Results for ammonia borane [AB], precursor [β -VBH(B3N2)] and alkali metal $\text{M}(\text{B3N2})$ salts: [Li(B3N2), Na(B3N2), K(B3N2), Rb(B3N2), Cs(B3N2)] at RT are shown for comparison.

	NH_3BH_3	VBH(B3N2)	M(B3N2) salts					$(\text{NH}_4)(\text{B3N2})\cdot 3(\text{B3N3})$
			Li(B3N2)	Na(B3N2)	K(B3N2)	Rb(B3N2)	Cs(B3N2)	
BH₂ triplet	–	–6.590	–6.743	–7.155	–7.499	–7.410	–7.792	–9.95 –11.78
	–	–8.184	–8.360	–8.582	–8.568	–8.424	–8.384	–10.40 –12.26
	–	–9.716	–9.966	–10.227	–9.591	–9.491	–9.042	–10.85 –12.70
position	–	–8.163	–8.356	–8.654	–8.553	–8.442	–8.406	–10.4 –12.3
1J (B,H)	–	100 Hz	103 Hz	99 Hz	101 Hz	100 Hz	101 Hz	101 Hz 102 Hz
freq.	96.32 MHz	64.16 MHz	96.32 MHz	96.32 MHz	96.32 MHz	96.32 MHz	160.48MHz	224.62 MHz

	NH_3BH_3	VBH(B3N2)	M(B3N2) salts					$(\text{NH}_4)(\text{B3N2})\cdot 3(\text{B3N3})$
			Li(B3N2)	Na(B3N2)	K(B3N2)	Rb(B3N2)	Cs(B3N2)	
BH₃ quartet	–18.184	–19.462	–20.465	–20.264	–20.613	–20.294	–20.279	–21.60
	–19.632	–20.933	–21.836	–21.693	–21.556	–21.226	–20.902	–22.01
	–21.144	–22.342	–23.314	–23.202	–22.499	–22.168	–21.479	–22.42
	–22.610	–23.752	–24.634	–24.582	–23.382	–23.105	–22.025	–22.83
position	–20.393	–21.622	–22.562	–22.435	–22.013	–21.698	–21.171	–22.21
1J (B,H)	95 Hz	91 Hz	90 Hz	91 Hz	89 Hz	90 Hz	94 Hz	91 HZ
freq.	96.32 MHz	64.16 MHz	96.32 MHz	96.32 MHz	96.32 MHz	96.32 MHz	160.48MHz	224.62 MHz

4. Table of bands appearing in the FTIR spectra of M(B3N2) salts and ammonia borane:

Table S4. Absorption bands detected in IR spectra (wavenumber [cm^{-1}]) of $\text{NH}_4(\text{B3N2})\cdot 3(\text{B3N3})$ at room temperature. Results for ammonia borane [AB] and alkali metal M(B3N2) salts: [Li(B3N2), Na(B3N2), K(B3N2), Rb(B3N2), Cs(B3N2)] at RT. Absorption bands of ammonia borane at RT are shown for comparison. (ν = stretching, δ = deformation: bending and torsional modes).

Band	NH_3BH_3	M(B3N2) salts					$(\text{NH}_4)(\text{B3N2})\cdot 3(\text{B3N3})$	
		Li(B3N2)	Na(B3N2)	K(B3N2)	Rb(B3N2)	Cs(B3N2)		
$\nu(\text{NH})$	3311 vs	3310 s	3302 vs	3305 vs	3308 m 3295 m	3313 w 3287 m	3306 vs 3288 vs 3268 sh	
	3253 vs	3273 m	3256 m	3261 m	3261 w 3252 w	3261 w 3235 m	3259 m 3239 m 3223 sh	
	3196 s							
$\nu(\text{BH})$				2420 sh			2439 sh 2407 s 2357 s 2317 vs 2302 sh	
	2347 vs	2350 vs 2322 s	2364 s 2315 s	2352 m	2390 sh 2346 s	2389 sh 2329 m		
	2289 s	2282 vs 2245 s	2286 vs	2304 s 2279 s 2259 s	2294 vs 2263 s 2248 sh 2204 sh	2291 vs	2260 m	
	2118 m					2248 s 2189 sh		
$\delta(\text{NH})$	1611 m				1617 vw		1604 sh 1572 w 1564 m 1556 m	
		1571 vs	1576 w 1556 m	1583 w 1568 m	1562 sh 1557 m	1579 vw 1565 w 1557 vw	1480 w 1428 w 1415 m 1392 m 1375 w	
$\delta(\text{BH})$	1163 vs	1283 m 1226 s 1201 s	1248 m	1244 m		1233 s 1206 m 1193 sh 1188 s	1259 m 1231 s 1205 s	1262 s 1244 s 1203 vs 1179 s
		1148 s 1135 m	1175 m	1194 sh 1182 m 1128 w	1193 sh 1167 s 1134 m	1171 s 1127 m	1168 sh 1134 m 1118 w	
			1129 vw	1074 m 1073 w	1065 w	1063 w	1078 w	
		1067 s	1044 m 1013 w	1055 m 999 w	1056 w 997 w	1038 w 1012 vw	1043 m 1001 w	1056 w 983 w
$\nu(\text{BN})$ and other		916 w	893 vw	893 vw 875 w	901 vw 873 vw	902 w 881 w	861 w	
		874 vw 799 vw	870 w 785 vw	781 vw 727 vw	854 vw 811 vw 727 vw	856 w 791 vw 723 vw	804 vw 749 w 711 w	

5. Table of bands appearing in the RAMAN spectra of M(B3N2) salts and ammonia borane:

Table S5. Absorption bands detected in Raman spectra (wavenumber [cm^{-1}]) of $\text{NH}_4(\text{B}_3\text{N}_2)\cdot 3(\text{B}_3\text{N}_3)$ at room temperature. Results for ammonia borane [AB] and alkali metal M(B3N2) salts: [Li(B3N2), Na(B3N2), K(B3N2), Rb(B3N2), Cs(B3N2)] at RT. Absorption bands of ammonia borane at RT are shown for comparison. (ν = stretching, δ = deformation: bending and torsional modes).

Band	NH_3BH_3	M(B3N2) salts					$(\text{NH}_4)(\text{B}_3\text{N}_2)\cdot 3(\text{B}_3\text{N}_3)$
		Li(B3N2)	Na(B3N2)	K(B3N2)	Rb(B3N2)	Cs(B3N2)	
$\nu(\text{NH})$					3304 sh	3307 sh	
	3314 m	3314 m	3302 s	3306 s	3293 w 3288 w	3303 w 3292 sh 3279 w	3307 m 3288 m
	3253 vs 3177 m	3272 s	3265 vs	3263 vs	3256 m 3245 m	3258 m 3232 m	3260 vs 3241 vs 3041 s
$\nu(\text{BH})$	2378 vs	2418 vw 2370 w	2403 w 2373 w	2382 m 2347 m	2379 m 2341 m	2379 m 2343 m	2475 sh 2442 w 2394 m 2320 vs 2261 s
	2284 vs	2282 m 2250 s	2275 s 2243 s 2214 sh	2301 s 2274 s	2291 vs 2243 vs	2286 vs 2250 vs	
		2166 vw		2186 sh	2192 sh		
$\delta(\text{NH})$	1598 m 1583 m	1567 m	1539 w 1519 vw	1649 vw 1585 vw 1569 vw	1608 vw 1565 w 1550 w	1645 vw 1566 w 1534 w	1578 s 1559 m
	1190 sh 1168 m 1069 vw	1281 w 1259 vw 1226 w 1206 m	1212 w	1227 w 1193 w 1168 w	1207 w 1188 m 1155 w 1122 vw 1056 vw	1206 sh 1183 m 1163 m 1036 vw	1201 w 1184 w 1173 w 1155 w 1102 w 1027 m 998 vs
$\delta(\text{BH})$		1010 w	1019 vw		1004 vw	993 w	
	$\nu(\text{BN})$ and other	895 vw 873 w 800 w 785 m 729w	856 vw 835 w 749 w 614 vw	892 vw 871 w 778 w	895 w 862 w 847 w 779 w 721 w 653 w 639 vw	915 w 899 vw 876 vw 851 w 783 vw 724 w 715 vw 643 vw	857 w 796 w 667 m 618 w 604 s

6. Comparison of FTIR and Raman spectra of alkali metal M(B3N2) salts:

FTIR and Raman spectra of $\text{NH}_4(\text{B3N2})/3(\text{B3N3})$ and alkali metal M(B3N2) salts: [Li(B3N2), Na(B3N2), K(B3N2), Rb(B3N2), Cs(B3N2)]. NH and BH stretching and NH bending regions highlighted and magnified in separate figures.

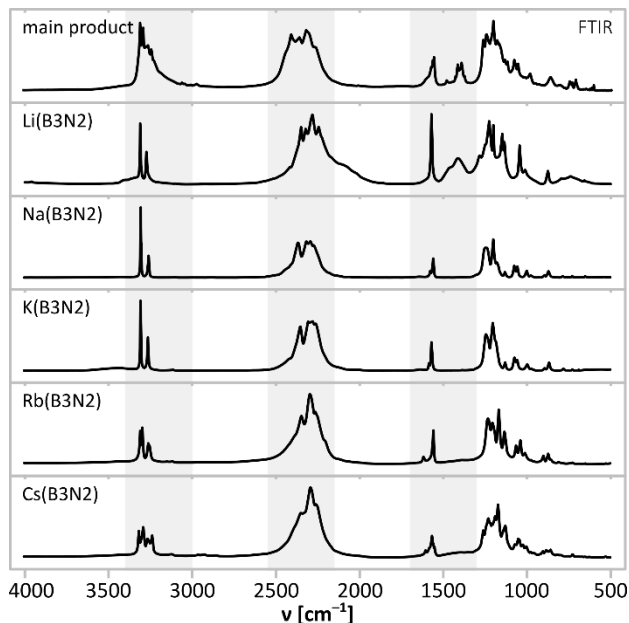


Fig. S6.1. Comparison of FTIR spectra of M(B3N2) salts.

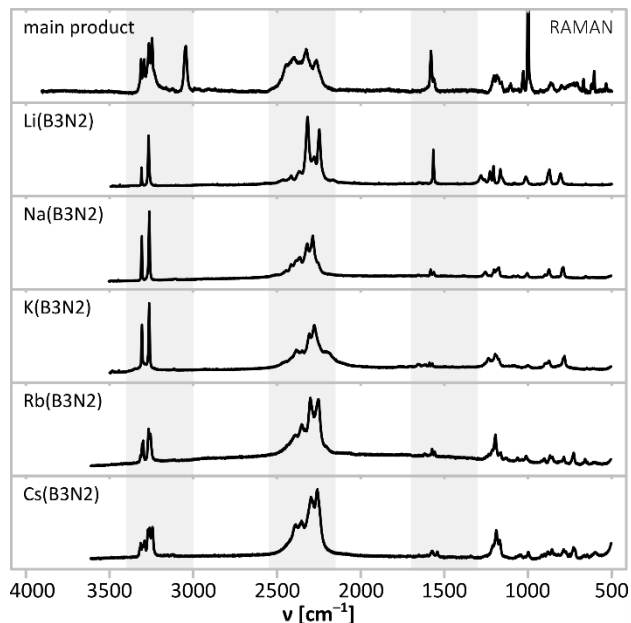


Fig. S6.2. Comparison of Raman spectra of M(B3N2) salts.

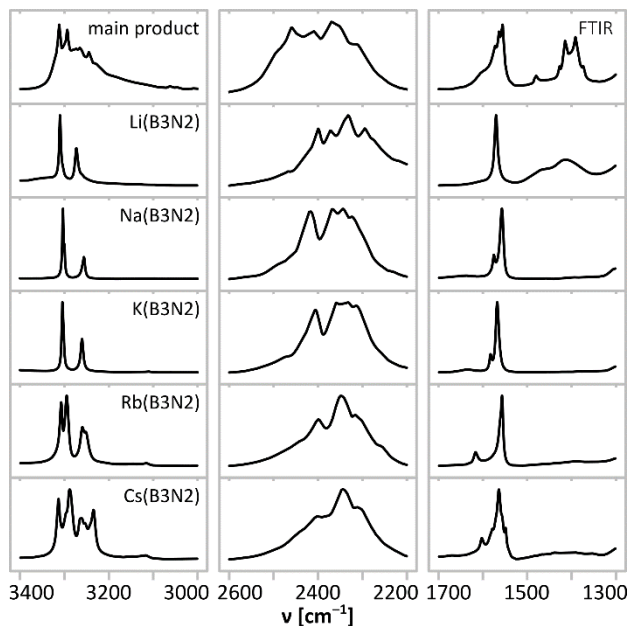


Fig. S6.3. Comparison of NH and BH stretching and NH bending regions of FTIR spectra of M(B3N2) salts.

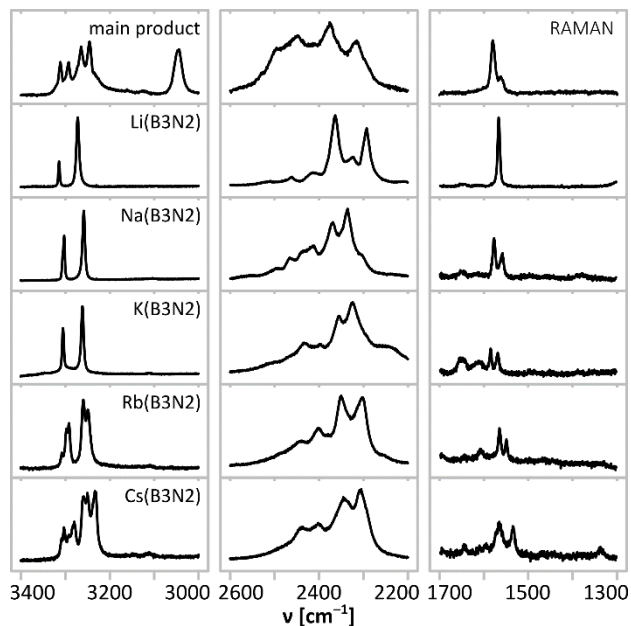


Fig. S6.4. Comparison of NH and BH stretching and NH bending regions of Raman spectra of M(B3N2) salts.

7. Thermal decomposition (TGA curves) of M(B3N2) salts:

The thermal decomposition of $\text{NH}_4(\text{B3N2})/3(\text{B3N3})$ and alkali metal M(B3N2) salts occurs at the temperature range of 120–180°C.

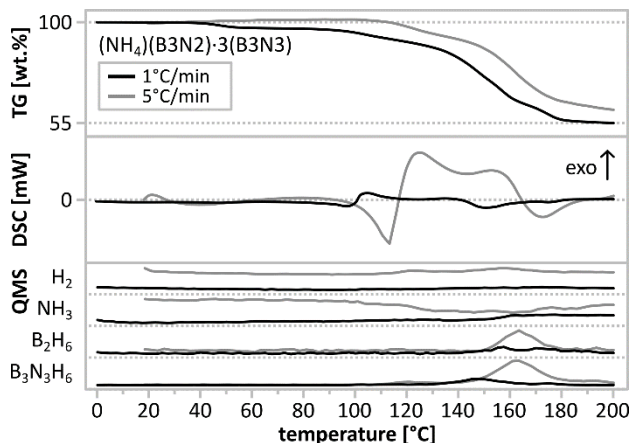


Fig.S7.1. TGA/DSC experiments of $(\text{NH}_4)(\text{B3N2}) \cdot 3(\text{B3N3})$ with scanning rates (1 K/min -black, 5 K/min -grey).

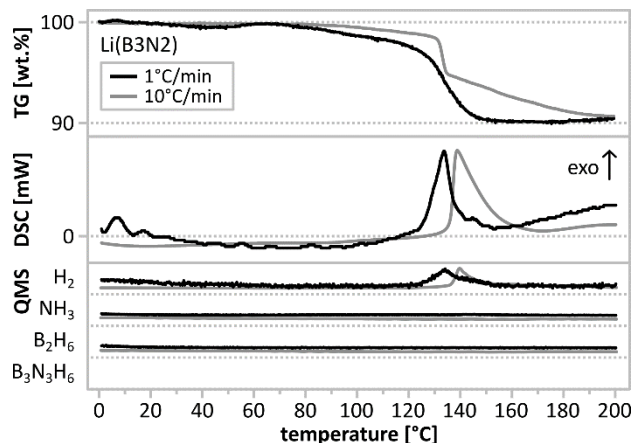


Fig.S7.2. TGA/DSC experiments of $\text{Li}(\text{B3N2})$ sample with different scanning rates (1 K/min -black, 10 K/min -grey).

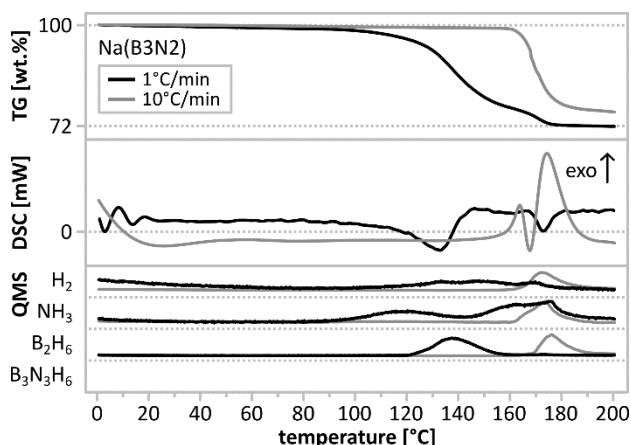


Fig.S7.3. TGA/DSC experiments of $\text{Na}(\text{B3N2})$ sample with different scanning rates (1 K/min -black, 10 K/min -grey).

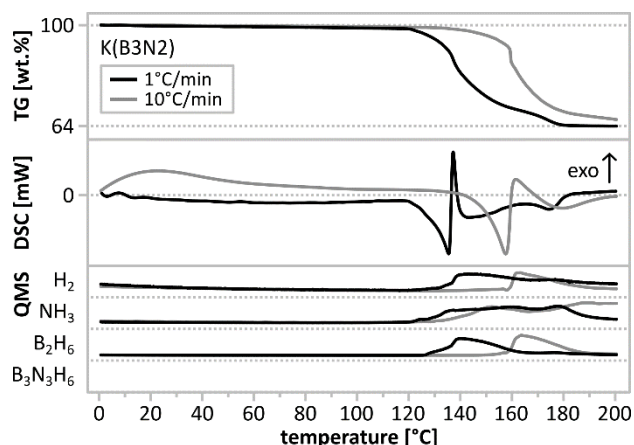


Fig.S7.4. TGA/DSC experiments of $\text{K}(\text{B3N2})$ sample with different scanning rates (1 K/min -black, 10 K/min -grey).

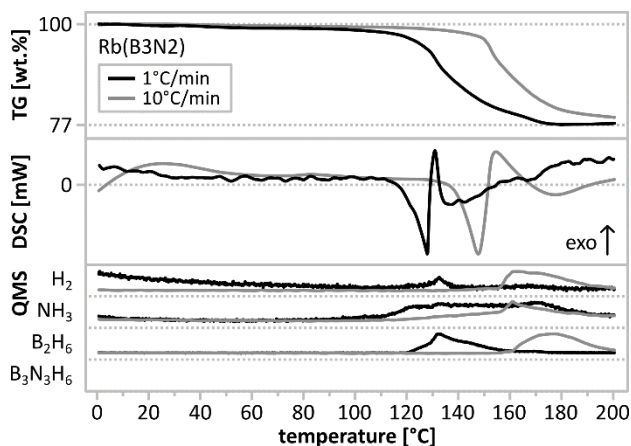


Fig.S7.5. TGA/DSC experiments of $\text{Rb}(\text{B3N2})$ sample with different scanning rates (1 K/min -black, 10 K/min -grey).

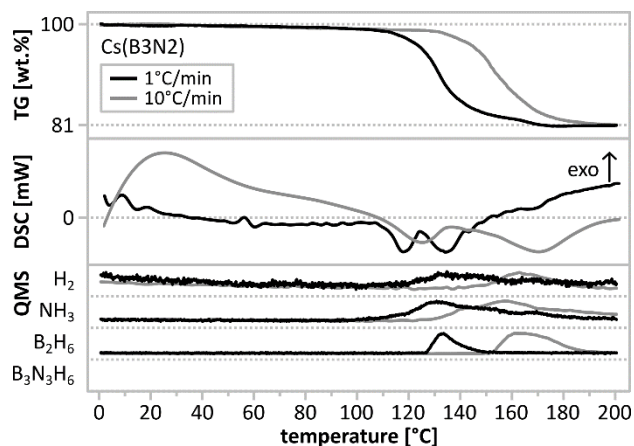


Fig.S7.6. TGA/DSC experiments of $\text{Cs}(\text{B3N2})$ sample with different scanning rates (1 K/min -black, 10 K/min -grey).

8. FTIR spectra of the products of thermal decomposition of M(B₃N₂) salts:

The thermal decomposition of (NH₄)(B₃N₂) leads to formation of boron nitride while decomposition of alkali metal M(B₃N₂) salts leads to formation of respective borohydrides.

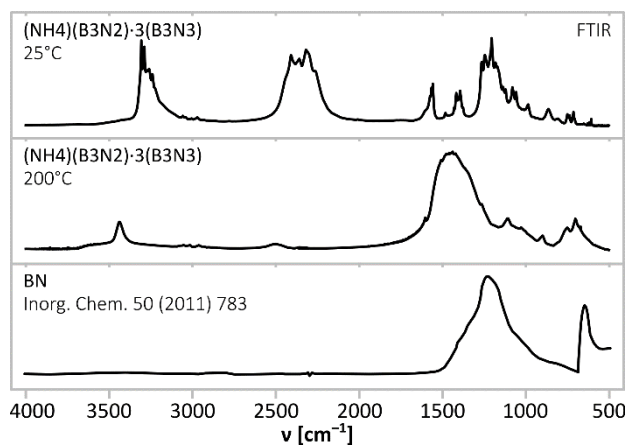


Fig. S8.1. FTIR spectra of the product of thermal decomposition of (NH₄)(B₃N₂)·3(B₃N₃) sample.

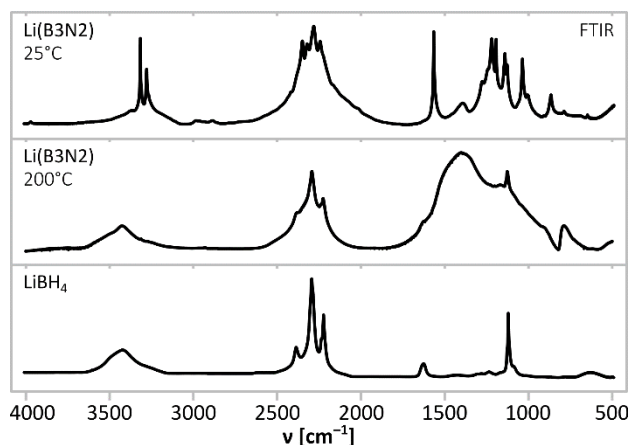


Fig. S8.2. FTIR spectra of the product of thermal decomposition of Li(B₃N₂) sample.

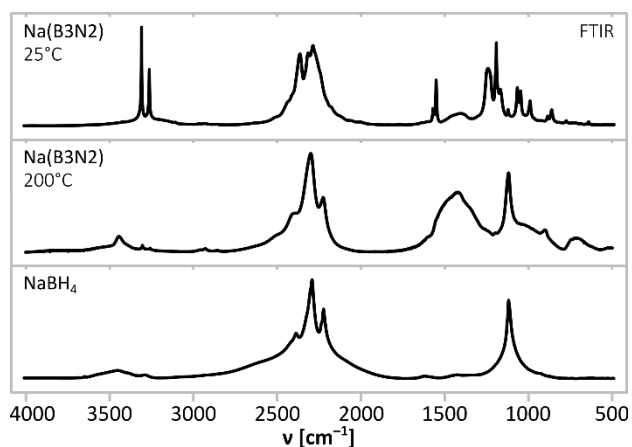


Fig. S8.3. FTIR spectra of the product of thermal decomposition of Na(B₃N₂) sample.

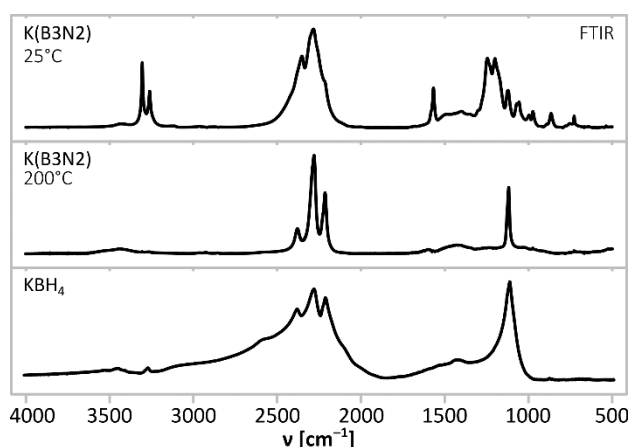


Fig. S8.4. FTIR spectra of the product of thermal decomposition of K(B₃N₂) sample.

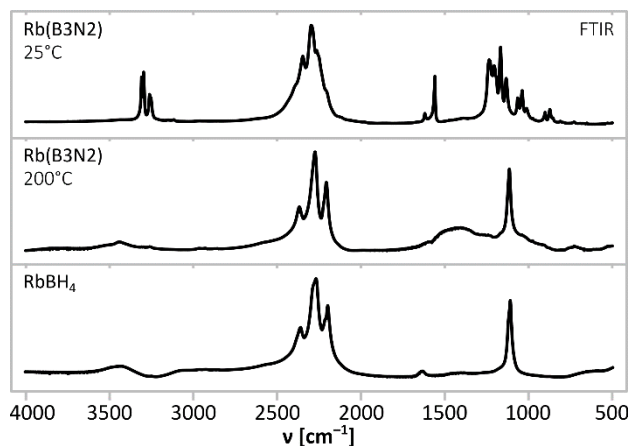


Fig. S8.5. FTIR spectra of the product of thermal decomposition of Rb(B₃N₂) sample.

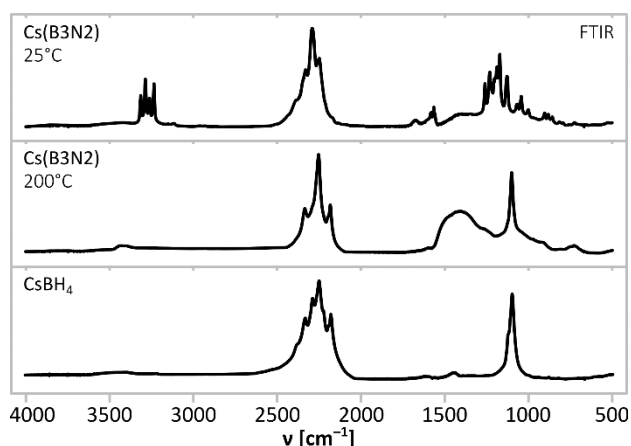


Fig. S8.6. FTIR spectra of the product of thermal decomposition of Cs(B₃N₂) sample.

9. Experimental crystal structure and Rietveld fit for $(\text{NH}_4)(\text{B3N2})\cdot 3(\text{B3N3})$:

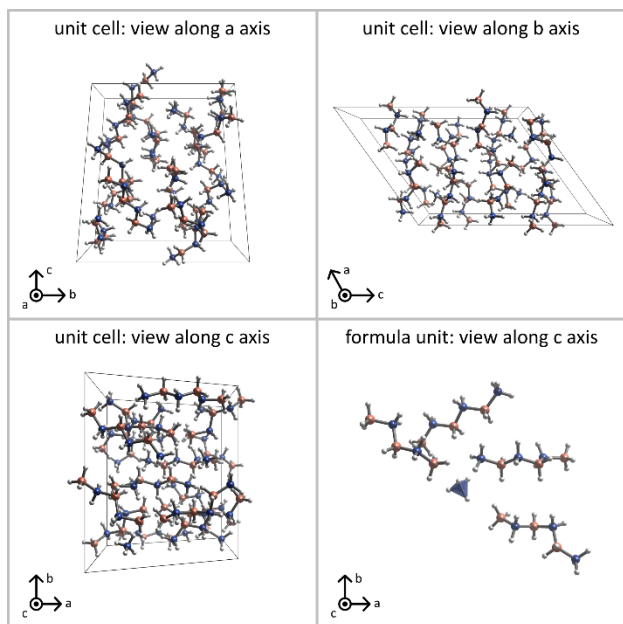


Fig. S9.1. Visualisation of the unit cell and formula unit of the main product: $(\text{NH}_4)(\text{B3N2})\cdot 3(\text{B3N3})$

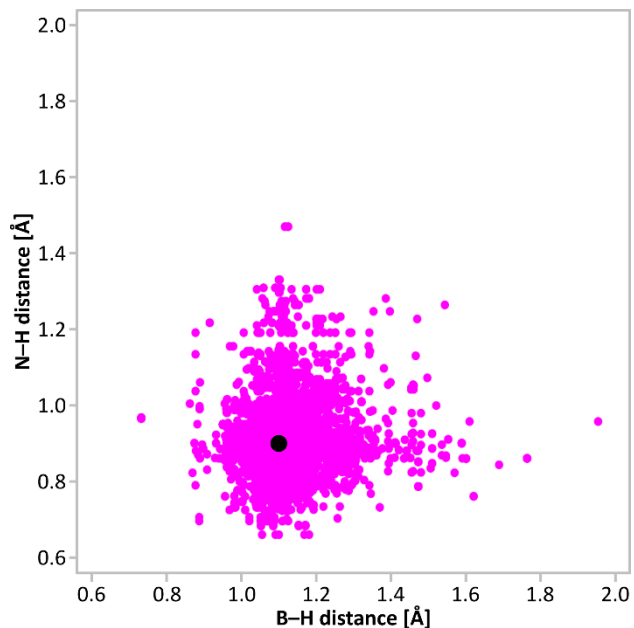


Fig. S9.2. Distribution of N-H and B-H distances in systems comprising both $[\text{NH}_x]$ and $[\text{BH}_x]$ groups found in structures in CSD database. Value of N-H and B-H distances in $(\text{NH}_4)(\text{B3N2})\cdot 3(\text{B3N3})$ marked with a dot.

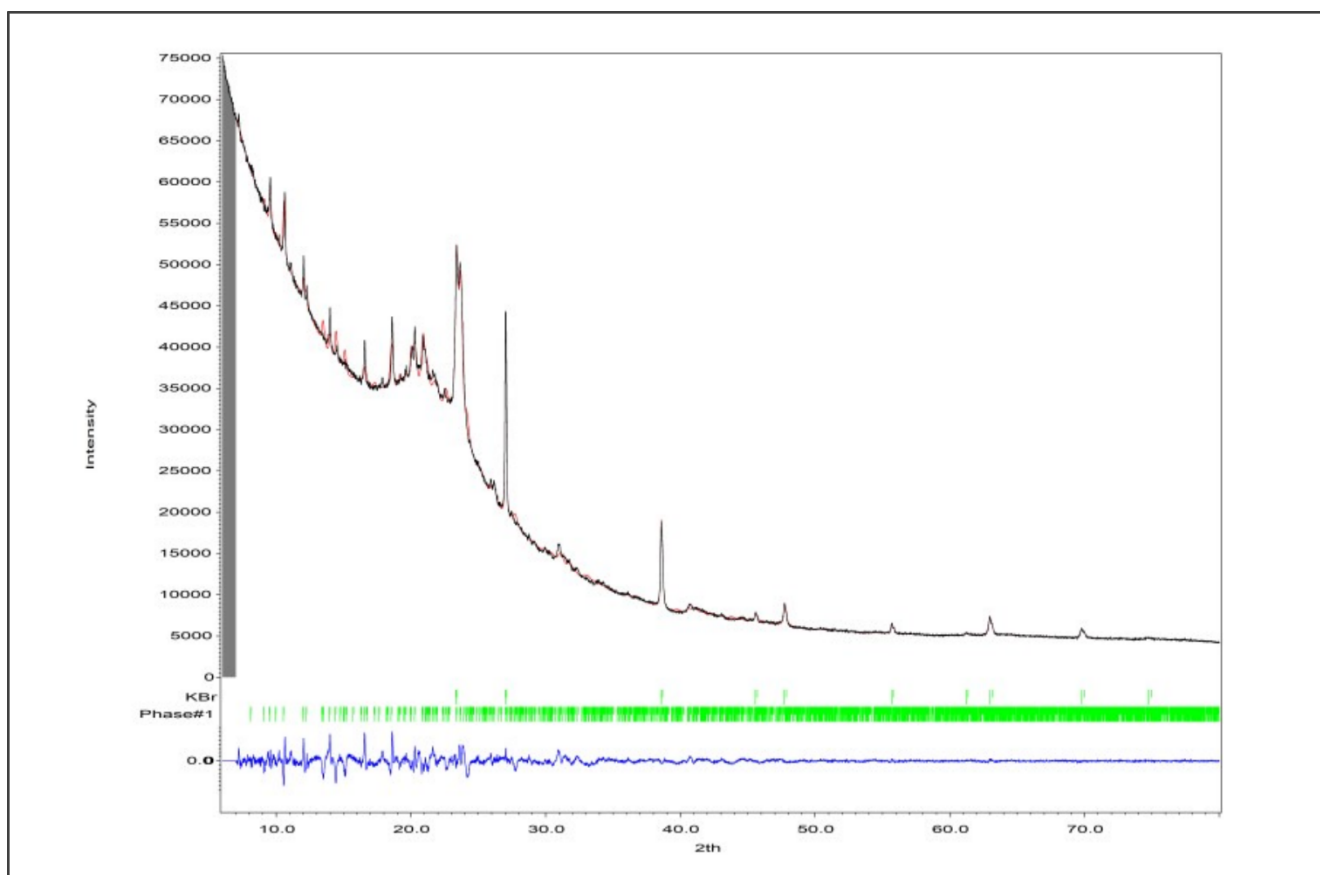


Fig. S9.3. Rietveld analysis of $(\text{NH}_4)(\text{B3N2})/3(\text{B3N3})$ powder pattern. $\text{CoK}_{\alpha 1,2}$, $\lambda = 1.78901 \text{ \AA}$.

10. Table with the closest H...H distances in the crystal structure of (NH₄)(B₃N₂)·3(B₃N₃):

Table S10. List of the closest H...H distances in experimental crystal structure of (NH₄)(B₃N₂)·3(B₃N₃). Listed only strong dihydrogen bonds, < 2 Å.

H atom1	H atom2	Length [Å]	Length-VdW [Å]	Neighboring groups
H8	H39	1.927	-0.473	B-H...H-N
H12	H29	1.928	-0.472	B-H...H-N
H6	H52	1.931	-0.469	B-H...H-N
H12	H53	1.935	-0.465	B-H...H-N
H15	H34	1.948	-0.452	B-H...H-B
H54	H42	1.949	-0.451	B-H...H-N
H1	H51	1.951	-0.449	B-H...H-N
H50	H64	1.971	-0.429	N-H...H-N
H19	H31	1.984	-0.416	B-H...H-B
H52	H64	1.987	-0.413	N-H...H-N
H17	H47	1.993	-0.407	B-H...H-N

11. Experimental and modelled NMR spectra for various possible compositions of the main product: NMR spectra were simulated for various discussed possible compositions of the main product to ease visual examination of the experimental spectra obtained by us and reported earlier by Ewing *et al.*, *Inorganic Chemistry* 52 (2013) 10690.

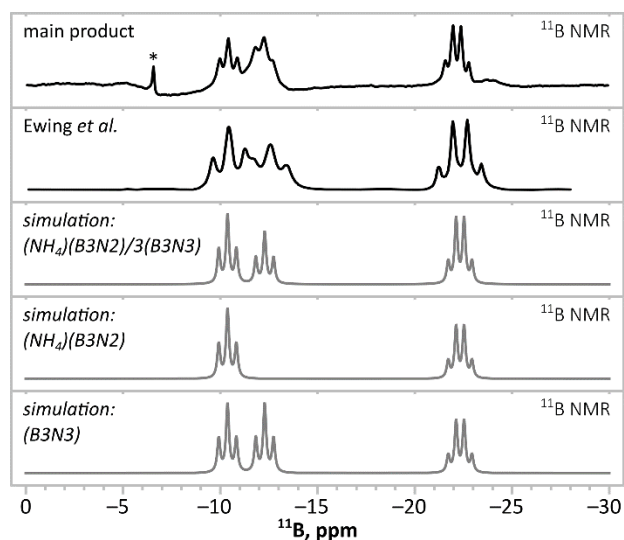


Fig. S11.1. Comparison of the experimental ^{11}B NMR spectra obtained here and reported by Ewing *et al.* (*Inorganic Chemistry* 52 (2013) 10690) with spectra simulated for various possible compositions of the main product: $(\text{NH}_4)(\text{B}_3\text{N}_2)\cdot 3(\text{B}_3\text{N}_3)$, $(\text{NH}_4)(\text{B}_3\text{N}_2)$ and (B_3N_3) .

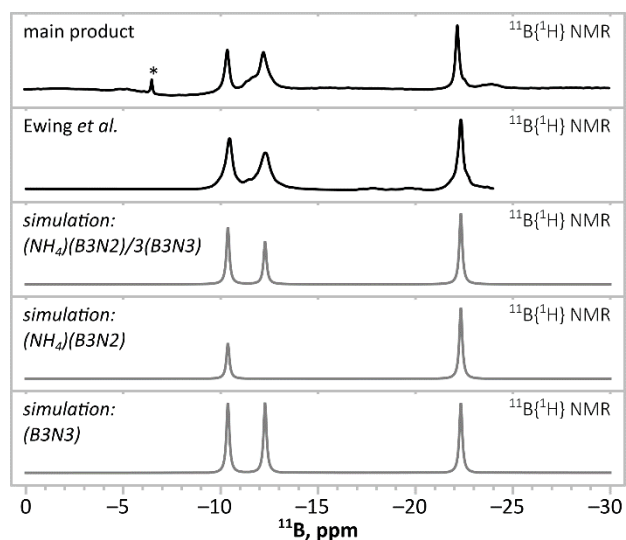


Fig. S11.2. Comparison of the experimental $^{11}\text{B}\{^1\text{H}\}$ NMR spectra obtained here and reported by Ewing *et al.* (*Inorganic Chemistry* 52 (2013) 10690) with spectra simulated for various possible compositions of the main product: $(\text{NH}_4)(\text{B}_3\text{N}_2)\cdot 3(\text{B}_3\text{N}_3)$, $(\text{NH}_4)(\text{B}_3\text{N}_2)$ and (B_3N_3) .

12. Results of DFT optimisation of modelled crystal structures:

NH₄(BH₃NH₂BH₂NH₂BH₃):3(NH₃BH₂NH₂BH₂NH₂BH₃), unit cell optimised

```
data_31_500eV\fine+cell
_audit_creation_date      2022-03-22
_audit_creation_method    'Materials Studio'
_symmetry_space_group_name_H-M  'P21/C'
_symmetry_Int_Tables_number  14
_symmetry_cell_setting    monoclinic
loop_
_symmetry_equiv_pos_as_xyz
  x,y,z
  -x,y+1/2,-z+1/2
  -x,-y,-z
  x,-y+1/2,z+1/2
_cell_length_a            13.2114
_cell_length_b            13.9512
_cell_length_c            19.0116
_cell_angle_alpha         90.0000
_cell_angle_beta          130.4617
_cell_angle_gamma         90.0000
loop_
_atom_site_label
_atom_site_type_symbol
_atom_site_fract_x
_atom_site_fract_y
_atom_site_fract_z
_atom_site_U_iso_or_equiv
_atom_site_adp_type
_atom_site_occupancy
B1  B  0.70821  0.11494  0.70797  0.05000  Uiso  1.00
N1  N  0.76629  0.14302  0.80732  0.05000  Uiso  1.00
B2  B  0.77307  0.25603  0.82169  0.05000  Uiso  1.00
N2  N  0.88332  0.27855  0.92649  0.05000  Uiso  1.00
B3  B  0.90995  0.38672  0.95751  0.05000  Uiso  1.00
H1  H  0.60523  0.15758  0.65051  0.05000  Uiso  1.00
H2  H  0.79337  0.12973  0.70200  0.05000  Uiso  1.00
H4  H  0.71177  0.11450  0.82381  0.05000  Uiso  1.00
H5  H  0.86071  0.11477  0.85440  0.05000  Uiso  1.00
H6  H  0.80153  0.29445  0.77863  0.05000  Uiso  1.00
H7  H  0.66525  0.28348  0.79429  0.05000  Uiso  1.00
H8  H  0.97286  0.25206  0.94872  0.05000  Uiso  1.00
H9  H  0.86665  0.24060  0.96452  0.05000  Uiso  1.00
H10 H  0.97588  0.38896  1.04154  0.05000  Uiso  1.00
H11 H  0.80194  0.42592  0.91975  0.05000  Uiso  1.00
H12 H  0.97000  0.42553  0.93710  0.05000  Uiso  1.00
B4  B  0.41303  0.33205  0.60553  0.05000  Uiso  1.00
N3  N  0.27925  0.35690  0.50627  0.05000  Uiso  1.00
B5  B  0.15136  0.33856  0.49619  0.05000  Uiso  1.00
N4  N  0.15353  0.41316  0.55956  0.05000  Uiso  1.00
B6  B  0.06225  0.39383  0.58541  0.05000  Uiso  1.00
H13 H  0.42249  0.24605  0.61536  0.05000  Uiso  1.00
H15 H  0.42037  0.37241  0.66568  0.05000  Uiso  1.00
H16 H  0.27593  0.42579  0.48531  0.05000  Uiso  1.00
H17 H  0.27253  0.31420  0.45908  0.05000  Uiso  1.00
H18 H  0.15917  0.25731  0.52314  0.05000  Uiso  1.00
H19 H  0.05145  0.35051  0.41580  0.05000  Uiso  1.00
H20 H  0.13000  0.48023  0.52964  0.05000  Uiso  1.00
H21 H  0.25125  0.41791  0.61940  0.05000  Uiso  1.00
```

H22	H	-0.05515	0.39939	0.51583	0.05000	Uiso	1.00
H23	H	0.08380	0.45473	0.64012	0.05000	Uiso	1.00
H24	H	0.08547	0.31319	0.61846	0.05000	Uiso	1.00
B7	B	0.35945	0.56131	0.01225	0.05000	Uiso	1.00
N5	N	0.39871	0.66288	-0.00050	0.05000	Uiso	1.00
B8	B	0.35089	0.76107	0.01297	0.05000	Uiso	1.00
N6	N	0.43801	0.78284	0.11929	0.05000	Uiso	1.00
B9	B	0.43903	0.89230	0.14365	0.05000	Uiso	1.00
H25	H	0.40686	0.49856	-0.00341	0.05000	Uiso	1.00
H26	H	0.39674	0.55325	0.08984	0.05000	Uiso	1.00
H28	H	0.50119	0.66593	0.04116	0.05000	Uiso	1.00
H29	H	0.36892	0.66512	-0.06589	0.05000	Uiso	1.00
H30	H	0.36881	0.82505	-0.02191	0.05000	Uiso	1.00
H31	H	0.23334	0.75618	-0.02405	0.05000	Uiso	1.00
H32	H	0.53513	0.76316	0.15269	0.05000	Uiso	1.00
H33	H	0.40908	0.74092	0.14813	0.05000	Uiso	1.00
H34	H	0.50214	0.93738	0.12797	0.05000	Uiso	1.00
H35	H	0.32535	0.92289	0.09508	0.05000	Uiso	1.00
H36	H	0.49200	0.89920	0.22589	0.05000	Uiso	1.00
B10	B	1.12914	0.99464	0.79230	0.05000	Uiso	1.00
N7	N	1.08247	0.88703	0.78744	0.05000	Uiso	1.00
B11	B	0.92947	0.86664	0.70636	0.05000	Uiso	1.00
N8	N	0.88287	0.77045	0.72226	0.05000	Uiso	1.00
B12	B	0.72463	0.75969	0.65604	0.05000	Uiso	1.00
H37	H	1.08482	1.04747	0.81782	0.05000	Uiso	1.00
H38	H	1.25109	0.99819	0.84578	0.05000	Uiso	1.00
H39	H	1.08213	1.01873	0.71408	0.05000	Uiso	1.00
H40	H	1.10997	0.87212	0.85076	0.05000	Uiso	1.00
H41	H	1.13739	0.84084	0.78158	0.05000	Uiso	1.00
H42	H	0.90914	0.85943	0.63407	0.05000	Uiso	1.00
H43	H	0.86774	0.93227	0.70464	0.05000	Uiso	1.00
H44	H	0.92197	0.71094	0.71553	0.05000	Uiso	1.00
H45	H	0.91808	0.76911	0.78909	0.05000	Uiso	1.00
H46	H	0.68750	0.80414	0.69155	0.05000	Uiso	1.00
H47	H	0.67311	0.79488	0.58006	0.05000	Uiso	1.00
H48	H	0.69326	0.67556	0.64739	0.05000	Uiso	1.00
N9	N	0.53664	0.37064	0.61627	0.05000	Uiso	1.00
H50	H	0.54045	0.44470	0.61701	0.05000	Uiso	1.00
H51	H	0.54125	0.34734	0.56683	0.05000	Uiso	1.00
H52	H	0.62319	0.34723	0.67920	0.05000	Uiso	1.00
N10	N	0.20232	0.54959	-0.06080	0.05000	Uiso	1.00
H53	H	0.15399	0.57777	-0.03889	0.05000	Uiso	1.00
H54	H	0.17501	0.47816	-0.07588	0.05000	Uiso	1.00
H55	H	0.15962	0.57929	-0.12419	0.05000	Uiso	1.00
N11	N	0.67472	0.00314	0.69163	0.05000	Uiso	1.00
H57	H	0.65387	-0.01839	0.63157	0.05000	Uiso	1.00
H58	H	0.75445	-0.03858	0.74368	0.05000	Uiso	1.00
H59	H	0.59194	-0.01451	0.68348	0.05000	Uiso	1.00
N12	N	0.23793	0.07365	0.68214	0.05000	Uiso	1.00
H61	H	0.21085	0.01630	0.63715	0.05000	Uiso	1.00
H62	H	0.19238	0.13480	0.64331	0.05000	Uiso	1.00
H63	H	0.34093	0.08208	0.72959	0.05000	Uiso	1.00
H64	H	0.20121	0.05757	0.71582	0.05000	Uiso	1.00

NH₄(BH₃NH₂BH₂NH₂BH₃), unit cell optimised

data_30_from00_noH-Hadd_500eV\fine+cell

_audit_creation_date 2022-03-22
_audit_creation_method 'Materials Studio'
_symmetry_space_group_name_H-M 'P21/C'
_symmetry_Int_Tables_number 14
_symmetry_cell_setting monoclinic

loop_

_symmetry_equiv_pos_as_xyz

x,y,z
-x,y+1/2,-z+1/2
-x,-y,-z
x,-y+1/2,z+1/2

_cell_length_a 15.1296
_cell_length_b 14.0974
_cell_length_c 18.5157
_cell_angle_alpha 90.0000
_cell_angle_beta 134.1837
_cell_angle_gamma 90.0000

loop_

_atom_site_label
_atom_site_type_symbol
_atom_site_fract_x
_atom_site_fract_y
_atom_site_fract_z
_atom_site_U_iso_or_equiv
_atom_site_adp_type
_atom_site_occupancy

B1	B	0.66514	0.10694	0.69465	0.05000	Uiso	1.00
N1	N	0.71546	0.20346	0.75835	0.05000	Uiso	1.00
B2	B	0.85400	0.20822	0.86832	0.05000	Uiso	1.00
N2	B	0.91110	0.30099	0.95489	0.05000	Uiso	1.00
B3	N	1.01642	0.24767	1.06367	0.05000	Uiso	1.00
B4	B	0.58384	0.42106	0.65635	0.05000	Uiso	1.00
N3	N	0.48530	0.38527	0.65775	0.05000	Uiso	1.00
B5	B	0.43120	0.46721	0.67502	0.05000	Uiso	1.00
N4	N	0.30905	0.43511	0.64480	0.05000	Uiso	1.00
B6	B	0.19360	0.41548	0.52834	0.05000	Uiso	1.00
B7	B	0.23139	0.77848	-0.05771	0.05000	Uiso	1.00
N5	N	0.29779	0.79874	0.05453	0.05000	Uiso	1.00
B8	B	0.43371	0.76148	0.14552	0.05000	Uiso	1.00
N6	N	0.53044	0.80777	0.14794	0.05000	Uiso	1.00
B9	B	0.67184	0.78858	0.24664	0.05000	Uiso	1.00
B10	B	1.04876	0.97755	0.69603	0.05000	Uiso	1.00
N7	N	0.98926	0.87693	0.67794	0.05000	Uiso	1.00
B11	B	0.84730	0.88149	0.61679	0.05000	Uiso	1.00
N8	N	0.79452	0.78276	0.61159	0.05000	Uiso	1.00
B12	B	0.64739	0.78172	0.53724	0.05000	Uiso	1.00
N9	N	0.30421	1.02782	0.92396	0.05000	Uiso	1.00
N10	N	0.89991	0.38928	0.23582	0.05000	Uiso	1.00
N11	N	0.40411	-0.02701	0.53429	0.05000	Uiso	1.00
N12	N	0.16159	0.03439	0.59474	0.05000	Uiso	1.00
H25	H	0.57587	0.08165	0.67916	0.00000	Uiso	1.00
H26	H	0.74209	0.04326	0.74155	0.00000	Uiso	1.00
H27	H	0.63368	0.12074	0.61368	0.00000	Uiso	1.00
H28	H	0.65741	0.21604	0.76811	0.00000	Uiso	1.00
H29	H	0.69738	0.25979	0.71420	0.00000	Uiso	1.00
H30	H	0.92670	0.20886	0.85760	0.00000	Uiso	1.00
H31	H	0.87080	0.13194	0.90858	0.00000	Uiso	1.00

H32	H	0.84498	0.34518	0.96014	0.00000	Uiso	1.00
H33	H	0.96760	0.36208	0.95162	0.00000	Uiso	1.00
H34	H	1.08626	0.28808	1.12530	0.00000	Uiso	1.00
H35	H	1.05800	0.19576	1.05622	0.00000	Uiso	1.00
H36	H	0.97446	0.21306	1.08218	0.00000	Uiso	1.00
H37	H	0.54476	0.49423	0.60574	0.00000	Uiso	1.00
H38	H	0.60038	0.36151	0.61857	0.00000	Uiso	1.00
H39	H	0.67976	0.43811	0.74197	0.00000	Uiso	1.00
H40	H	0.52471	0.33553	0.71369	0.00000	Uiso	1.00
H41	H	0.41727	0.34701	0.59332	0.00000	Uiso	1.00
H42	H	0.40227	0.53202	0.61842	0.00000	Uiso	1.00
H43	H	0.51021	0.49321	0.76251	0.00000	Uiso	1.00
H44	H	0.28544	0.48737	0.66769	0.00000	Uiso	1.00
H45	H	0.32357	0.37640	0.68540	0.00000	Uiso	1.00
H46	H	0.10247	0.39780	0.51231	0.00000	Uiso	1.00
H47	H	0.21701	0.34798	0.50190	0.00000	Uiso	1.00
H48	H	0.17298	0.48714	0.48003	0.00000	Uiso	1.00
H49	H	0.23580	0.69217	-0.06386	0.00000	Uiso	1.00
H50	H	0.28267	0.81830	-0.07846	0.00000	Uiso	1.00
H51	H	0.12202	0.80402	-0.11675	0.00000	Uiso	1.00
H52	H	0.24488	0.76892	0.06495	0.00000	Uiso	1.00
H53	H	0.29626	0.87047	0.06438	0.00000	Uiso	1.00
H54	H	0.43438	0.67496	0.13879	0.00000	Uiso	1.00
H55	H	0.46301	0.78204	0.22402	0.00000	Uiso	1.00
H56	H	0.51767	0.88032	0.14098	0.00000	Uiso	1.00
H57	H	0.51530	0.78744	0.08665	0.00000	Uiso	1.00
H58	H	0.73769	0.83551	0.24300	0.00000	Uiso	1.00
H59	H	0.69524	0.70472	0.25101	0.00000	Uiso	1.00
H60	H	0.69072	0.81080	0.32069	0.00000	Uiso	1.00
H61	H	0.98211	1.02676	0.62065	0.00000	Uiso	1.00
H62	H	1.15010	0.96615	0.72590	0.00000	Uiso	1.00
H63	H	1.06616	1.01664	0.76417	0.00000	Uiso	1.00
H64	H	1.03969	0.84687	0.74802	0.00000	Uiso	1.00
H65	H	1.00510	0.83410	0.64268	0.00000	Uiso	1.00
H66	H	0.79154	0.90640	0.53074	0.00000	Uiso	1.00
H67	H	0.83251	0.93665	0.65811	0.00000	Uiso	1.00
H68	H	0.83316	0.76230	0.68178	0.00000	Uiso	1.00
H69	H	0.81562	0.73071	0.58623	0.00000	Uiso	1.00
H70	H	0.61644	0.70373	0.54393	0.00000	Uiso	1.00
H71	H	0.60103	0.79436	0.45185	0.00000	Uiso	1.00
H72	H	0.61714	0.84255	0.56348	0.00000	Uiso	1.00
H73	H	0.23237	1.01081	0.84819	0.00000	Uiso	1.00
H74	H	0.37678	0.98260	0.95540	0.00000	Uiso	1.00
H75	H	0.33389	1.09739	0.93189	0.00000	Uiso	1.00
H76	H	0.27302	1.02156	0.95924	0.00000	Uiso	1.00
H77	H	0.92845	0.34726	0.29651	0.00000	Uiso	1.00
H78	H	0.85564	0.34756	0.17184	0.00000	Uiso	1.00
H79	H	0.83467	0.43444	0.22113	0.00000	Uiso	1.00
H80	H	0.97006	0.42799	0.25162	0.00000	Uiso	1.00
H81	H	0.40974	-0.08366	0.57357	0.00000	Uiso	1.00
H82	H	0.40191	-0.05445	0.48091	0.00000	Uiso	1.00
H83	H	0.32424	0.01191	0.49763	0.00000	Uiso	1.00
H84	H	0.47946	0.01857	0.58567	0.00000	Uiso	1.00
H85	H	0.17156	-0.02595	0.56907	0.00000	Uiso	1.00
H86	H	0.08359	0.07275	0.53422	0.00000	Uiso	1.00
H87	H	0.14981	0.01190	0.64117	0.00000	Uiso	1.00
H88	H	0.23755	0.07955	0.63623	0.00000	Uiso	1.00

(NH₃BH₂NH₂BH₂NH₂BH₃), unit cell optimised

data_32_500eV\fine+cell

_audit_creation_date 2022-04-05
_audit_creation_method 'Materials Studio'
_symmetry_space_group_name_H-M 'P21/C'
_symmetry_Int_Tables_number 14
_symmetry_cell_setting monoclinic

loop_

_symmetry_equiv_pos_as_xyz

x,y,z
-x,y+1/2,-z+1/2
-x,-y,-z
x,-y+1/2,z+1/2

_cell_length_a 14.0521
_cell_length_b 12.5784
_cell_length_c 19.2528
_cell_angle_alpha 90.0000
_cell_angle_beta 128.7292
_cell_angle_gamma 90.0000

loop_

_atom_site_label
_atom_site_type_symbol
_atom_site_fract_x
_atom_site_fract_y
_atom_site_fract_z
_atom_site_U_iso_or_equiv
_atom_site_adp_type
_atom_site_occupancy

B1	B	0.61234	0.14161	0.69593	0.05000	Uiso	1.00
N1	N	0.74985	0.13798	0.78118	0.05000	Uiso	1.00
B2	B	0.80335	0.24827	0.83148	0.05000	Uiso	1.00
N2	N	0.94601	0.24008	0.90513	0.05000	Uiso	1.00
B3	B	1.00612	0.33672	0.97390	0.05000	Uiso	1.00
H1	H	0.54946	0.17792	0.71315	0.05000	Uiso	1.00
H2	H	0.60187	0.18975	0.63663	0.05000	Uiso	1.00
H4	H	0.76311	0.08260	0.82641	0.05000	Uiso	1.00
H5	H	0.80196	0.11174	0.76378	0.05000	Uiso	1.00
H6	H	0.78333	0.31438	0.77695	0.05000	Uiso	1.00
H7	H	0.75652	0.27053	0.86549	0.05000	Uiso	1.00
H8	H	0.98548	0.23333	0.87482	0.05000	Uiso	1.00
H9	H	0.97069	0.17067	0.94111	0.05000	Uiso	1.00
H10	H	1.00173	0.31692	1.03399	0.05000	Uiso	1.00
H11	H	0.95188	0.41887	0.93541	0.05000	Uiso	1.00
H12	H	1.11486	0.34492	1.00700	0.05000	Uiso	1.00
B4	B	0.50969	0.43569	0.71360	0.05000	Uiso	1.00
N3	N	0.46702	0.38819	0.62292	0.05000	Uiso	1.00
B5	B	0.33020	0.34237	0.55254	0.05000	Uiso	1.00
N4	N	0.25702	0.34528	0.59044	0.05000	Uiso	1.00
B6	B	0.17134	0.44485	0.56525	0.05000	Uiso	1.00
H13	H	0.50674	0.36814	0.75773	0.05000	Uiso	1.00
H15	H	0.45024	0.51405	0.70061	0.05000	Uiso	1.00
H16	H	0.47623	0.44544	0.58905	0.05000	Uiso	1.00
H17	H	0.52384	0.32667	0.63483	0.05000	Uiso	1.00
H18	H	0.33803	0.24984	0.53711	0.05000	Uiso	1.00
H19	H	0.27691	0.39738	0.48626	0.05000	Uiso	1.00
H20	H	0.31598	0.33436	0.65830	0.05000	Uiso	1.00
H21	H	0.20393	0.27761	0.56705	0.05000	Uiso	1.00
H22	H	0.22991	0.52690	0.58489	0.05000	Uiso	1.00
H23	H	0.12913	0.44167	0.60495	0.05000	Uiso	1.00

H24	H	0.08772	0.44511	0.48540	0.05000	Uiso	1.00
B7	B	0.27345	0.57022	-0.00885	0.05000	Uiso	1.00
N5	N	0.26635	0.66818	-0.06284	0.05000	Uiso	1.00
B8	B	0.22211	0.77997	-0.05360	0.05000	Uiso	1.00
N6	N	0.33300	0.83259	0.03608	0.05000	Uiso	1.00
B9	B	0.44363	0.86757	0.03827	0.05000	Uiso	1.00
H25	H	0.31804	0.49323	-0.01834	0.05000	Uiso	1.00
H26	H	0.33068	0.59327	0.06945	0.05000	Uiso	1.00
H28	H	0.34950	0.68144	-0.04834	0.05000	Uiso	1.00
H29	H	0.20852	0.64938	-0.12983	0.05000	Uiso	1.00
H30	H	0.19464	0.83592	-0.11562	0.05000	Uiso	1.00
H31	H	0.13695	0.76681	-0.05285	0.05000	Uiso	1.00
H32	H	0.36163	0.78334	0.08860	0.05000	Uiso	1.00
H33	H	0.29991	0.89825	0.04691	0.05000	Uiso	1.00
H34	H	0.41205	0.94339	-0.01110	0.05000	Uiso	1.00
H35	H	0.53224	0.88970	0.11504	0.05000	Uiso	1.00
H36	H	0.47107	0.79357	0.01180	0.05000	Uiso	1.00
B10	B	1.01084	1.09682	0.78046	0.05000	Uiso	1.00
N7	N	1.00571	0.98490	0.81574	0.05000	Uiso	1.00
B11	B	0.89496	0.91200	0.74411	0.05000	Uiso	1.00
N8	N	0.88698	0.81275	0.79116	0.05000	Uiso	1.00
B12	B	0.76080	0.75282	0.73529	0.05000	Uiso	1.00
H37	H	0.91116	1.14046	0.73976	0.05000	Uiso	1.00
H38	H	1.08492	1.15377	0.84346	0.05000	Uiso	1.00
H39	H	1.03831	1.08470	0.73181	0.05000	Uiso	1.00
H40	H	1.00795	0.99774	0.86972	0.05000	Uiso	1.00
H41	H	1.08598	0.94429	0.84318	0.05000	Uiso	1.00
H42	H	0.90823	0.88165	0.69059	0.05000	Uiso	1.00
H43	H	0.79993	0.96281	0.70640	0.05000	Uiso	1.00
H44	H	0.95736	0.76075	0.81376	0.05000	Uiso	1.00
H45	H	0.90141	0.83918	0.84788	0.05000	Uiso	1.00
H46	H	0.68411	0.81054	0.72636	0.05000	Uiso	1.00
H48	H	0.76990	0.66919	0.77091	0.05000	Uiso	1.00
N9	N	0.64892	0.47383	0.77073	0.05000	Uiso	1.00
H50	H	0.65955	0.53699	0.74190	0.05000	Uiso	1.00
H51	H	0.70708	0.41277	0.78183	0.05000	Uiso	1.00
H52	H	0.68082	0.49842	0.83280	0.05000	Uiso	1.00
N10	N	0.13759	0.54192	-0.04916	0.05000	Uiso	1.00
H53	H	0.10005	0.59620	-0.03170	0.05000	Uiso	1.00
H54	H	0.12833	0.46828	-0.02971	0.05000	Uiso	1.00
H55	H	0.07927	0.54020	-0.11808	0.05000	Uiso	1.00
N11	N	0.56770	0.02149	0.66238	0.05000	Uiso	1.00
H57	H	0.48257	0.01895	0.60065	0.05000	Uiso	1.00
H58	H	0.62717	-0.02152	0.65896	0.05000	Uiso	1.00
H59	H	0.55927	-0.01953	0.70490	0.05000	Uiso	1.00
N12	N	0.27916	0.22761	0.86024	0.05000	Uiso	1.00
H61	H	0.36599	0.19486	0.90001	0.05000	Uiso	1.00
H63	H	0.28219	0.29363	0.89304	0.05000	Uiso	1.00
H64	H	0.22046	0.17569	0.85841	0.05000	Uiso	1.00

13. Crystal structure (VBH)[B(C₆H₅)₄]

Table 13.1. Crystal structure parameters of (C₁₈H₃₉N₄PH)[B(C₆H₅)₄].

Compound	(C ₁₈ H ₃₉ N ₄ PH)[B(C ₆ H ₅) ₄]
K _α (Å)	1.54184 (Cu)
Temperature (K)	100(2)
Space group	<i>P</i> 1
Z	4
<i>a</i> (Å)	11.7376(3)
<i>b</i> (Å)	19.5388(5)
<i>c</i> (Å)	20.5479(4)
α (°)	61.751(2)
β (°)	73.618(2)
γ (°)	89.605(2)
<i>V</i> (Å ³)	3937.71(18)
$\rho_{calc.}$ (g cm ⁻³)	1.118
$\mu_{exp.}$ (mm ⁻¹)	0.856
ϑ_{max} (°)	75.2030
<i>R</i> ₁	0.0695
<i>wR</i> ₂	0.2094
<i>Goof</i>	1.048
Crystal size (mm×mm×mm)	0.06 x 0.16 x 0.20
Crystal colour	colorless
CCDC No.	

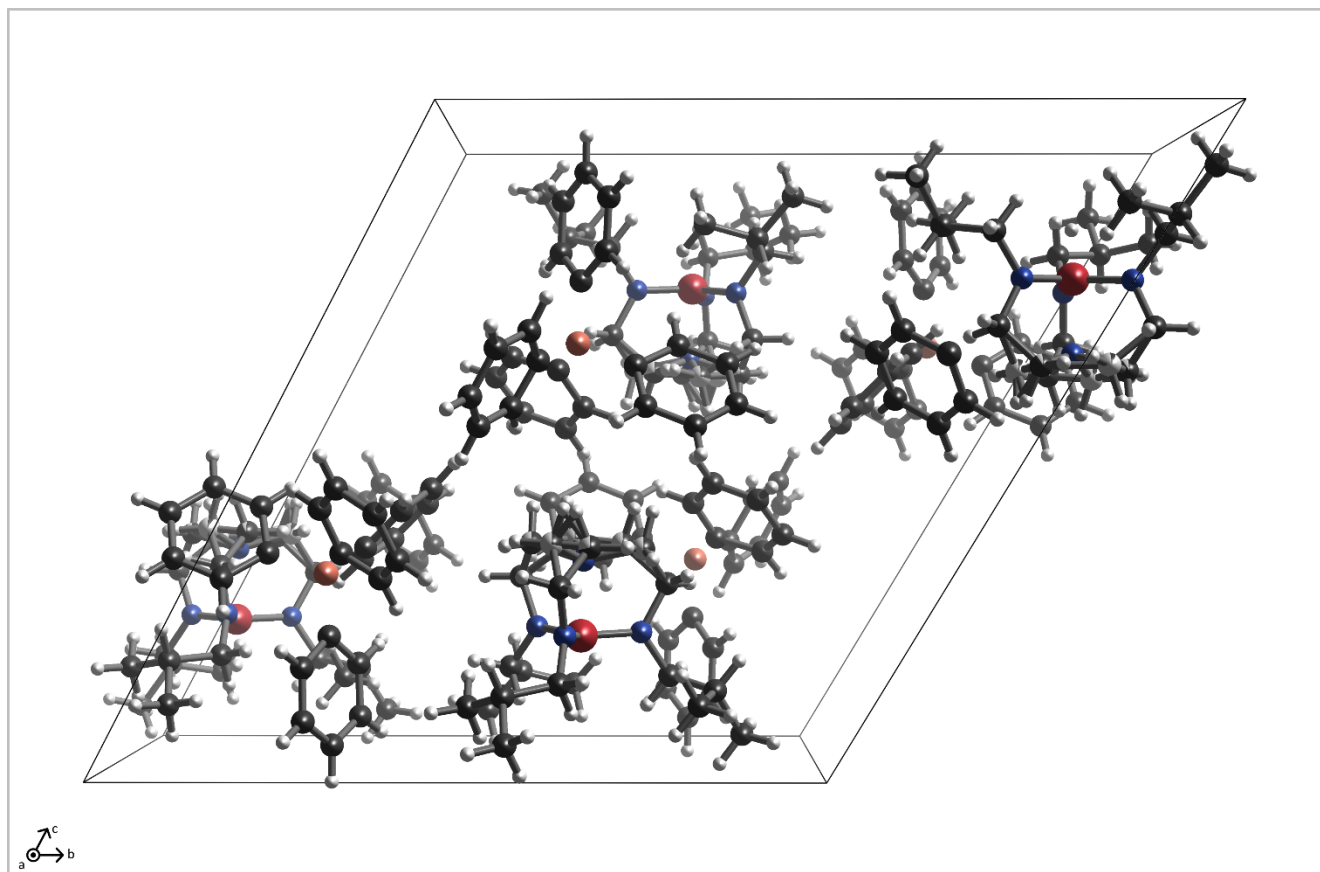


Fig. S13.2. Visualisation of the unit cell of the side product: (C₁₈H₃₉N₄PH)[B(C₆H₅)₄].